MATHEMATICAL MODELING OF FLOWBACK WATER TREATMENT USING REVERSE OSMOSIS AND NANOFILTRATION TECHNOLOGIES

by

Pedro Henrique Casa Grande Rosa

Bachelor's Degree, Universidade Federal do Espírito Santo, 2012

Submitted to the Graduate Faculty of

Swanson School of Engineering in partial fulfillment

of the requirements for the degree of

Master of Science

University of Pittsburgh

2016

UNIVERSITY OF PITTSBURGH

SWANSON SCHOOL OF ENGINEERING

This thesis was presented

by

Pedro Henrique Casa Grande Rosa

It was defended on

April 27, 2016

and approved by

George E. Klinzing, Ph.D., Professor, Department of Chemical and Petroleum Engineering

Robert M. Enick, Ph.D., Professor, Department of Chemical and Petroleum Engineering

Thesis Advisor: Badie I. Morsi, Ph.D., Professor, Department of Chemical and Petroleum Engineering

MATHEMATICAL MODELING OF FLOWBACK WATER TREATMENT USING REVERSE OSMOSIS AND NANOFILTRATION TECHNOLOGIES

Pedro Henrique Casa Grande Rosa, M.S.

University of Pittsburgh, 2016

The main objective of this study is to assess, through mathematical modeling, the potential use and feasibility of deploying nanofiltration and reverse osmosis technologies in the treatment of flowback water. Field data of flowback water flow rates and chemical composition were used in the models in order to provide an accurate assessment of each technology. Operating conditions based on the current commercial reverse osmosis and nanofiltration membranes for water treatment were also considered. Mathematical models for the reverse osmosis and nanofiltration processes were developed to assess the performance of these processes in the treatment of flowback water produced during the hydraulic fracturing for natural gas production from shale plays. The models, based on the mass balance and thermodynamics, were verified and implemented in Matlab version R2015.

The models were used to perform a sensitivity analysis for the two processes in order to determine the effect of the operating variables on the membrane performance in terms of solute concentration and filtration time. For the reverse osmosis, it was found that pressure drop, inlet flow rate and membrane area were the major parameters governing the process. For nanofiltration, on the other hand, pressure drop, reflection coefficient and membrane area were the most important parameters affecting the process performance.

The models were also used to assess and compare the performance of four different commercial reverse osmosis and three nanofiltration membranes using actual field data, such as inlet flowrate and flowback water composition. The predictions of the two models showed that the reverse osmosis was significantly superior to the nanofiltration membranes in the removal of Na^+ and Ca^{2+}. Nanofiltration membranes, however, exhibited higher removal efficiencies for Cl^- than that of the reverse osmosis membranes. This behavior was attributed primarily to the nature of both processes; since the reverse osmosis is mainly driven by the chemical potential of chlorine, whereas, the nanofiltration is controlled by the molecule size.

TABLE OF CONTENTS

LIST OF TABLES

LIST OF FIGURES

NOMENCLATURE

c	Concentration (kmol/m^3)
D_i	Diffusion coefficient (m^2/s)
J	Flux (kg/m^2 s)
k_m	Mass transfer coefficient (kg/m^2 s)
K	Partition coefficient across the RO membrane
K_c	Convective hindrance factor
l	Membrane thickness (m)
L_i	Coefficient of proportionality for the solution diffusion model (mol·s/m^3)
L_P	Pipe Length (m)
M_w	Molecular weight (g/mol)
p	Pressure (Pa)
R	Universal Gas Constant (J/mol-K)
T	Temperature (K)
x	Directional coordinate (m)
γ_i	Activity coefficient of component i
σ_o	Osmotic reflection coefficient
κ_A	Water permeability (g-m/mol-s)
κ_A'	Adjusted water permeability (s/m)
κ_B	Solute Permeability (g-m/mol-s)
δ	Boundary layer thickness
π	Osmotic pressure (Pa)
ω	Constant (kg/m^2 s)
ν_i	Molar volume of component i (m^3/mol)

μ_i	Chemical potential (J/mol)

Subscripts

A	Water
av	Average concentration in the membrane for nanofiltration
B	Solute
p	Permeate
m	Average concentration in the membrane for reverse osmosis
w	Wall

PREFACE

My special thanks:

To my academic and research advisor, Dr. Badie Morsi, for believing in my potential and for providing the support and the opportunity to work along with so many talented individuals, who helped me going through the whole period of preparation of this work sharing their kindness and experiences.

To Mr. Omar Basha, who is a huge collaborator in this project, for his selflessness, humbleness and for being always ready to help with his competence and incredible intelligence.

To my family, for all their love and support during this time, for their prayers and for reminding me that I will always have them to count on.

To my beloved grandfather, Valmiré, to whom this work is dedicated, in memoriam.

To my friends, for cheering me up and for making the distance from my family tolerable.

To the Coordination for the Improvement of Higher Education Personnel (CAPES), for the scholarship through the program Science-Without-Borders (Ciência sem Fronteiras), sponsored by the Brazilian Government.

To God, for His unconditional love.

1.0 INTRODUCTION

With recent advances in horizontal drilling and hydraulic fracturing (fracking) technologies, shale gas extraction is on the rise and is expected to continue to grow in the US and around the world. The United States Energy Information Administration (US-EIA) estimated that horizontal shale drilling will increase the total recoverable natural gas reserves by over 40% worldwide. The US-EIA also estimated that shale oil and gas are expected to play an important role in meeting the global energy demand, which was expected to increase 34% by 2035, driven by the expected increase of world economy and population [1]. Globally, 32% of the total estimated natural gas reserves are in shale formations, while 10% of the estimated oil reserves are in shale or tight formations [1]. In the US, the "shale revolution" has sparked a remarkable change in the gas industry. This revolution has been catalyzed by advances in horizontal drilling and fracking technologies. These technological advances have made shale an increasingly attractive natural gas source, allowing the US to ensure its energy independence and national security.

Shale gas is thought by experts to be plentiful in the US and many other countries around the world, such as Poland, France, South Africa, Libya, Algeria, Argentina, as Brazil, as shown in Figure 1. Figure 2 shows that the US has a large share of the world's recoverable shale oil and gas reserves, with 16.8% and 9.2%, respectively.

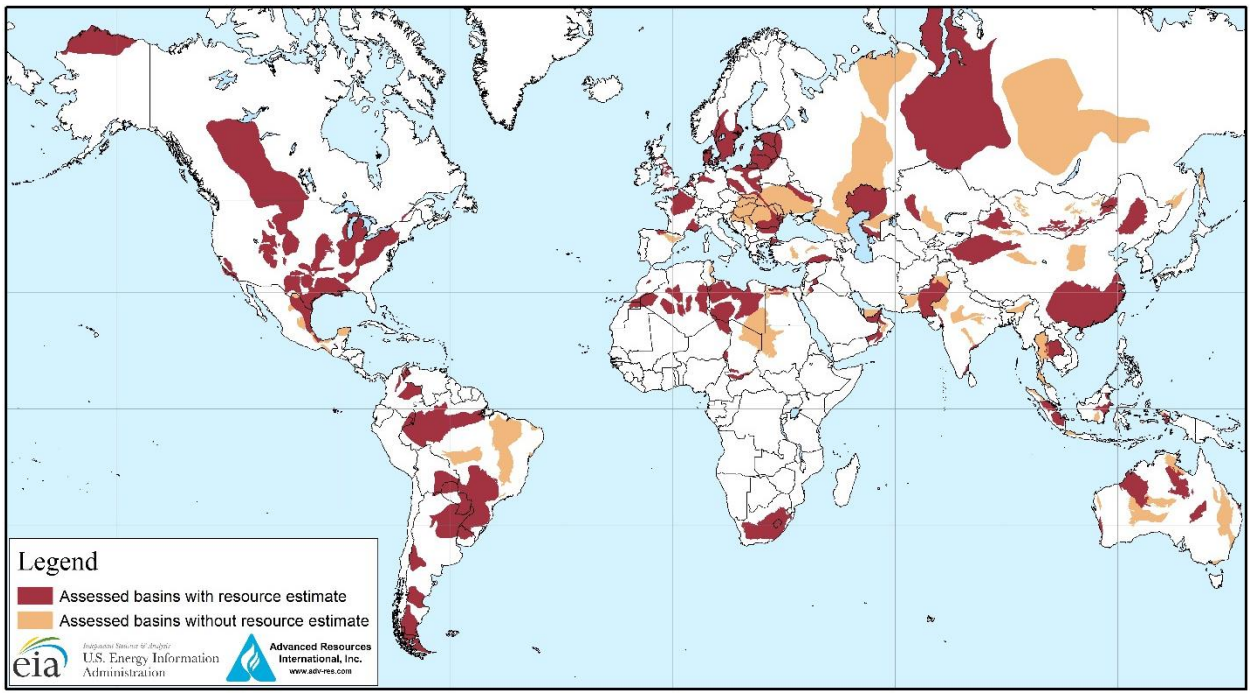

Figure 1: Map of basins with shale and oil gas formations, May 2013 [1]

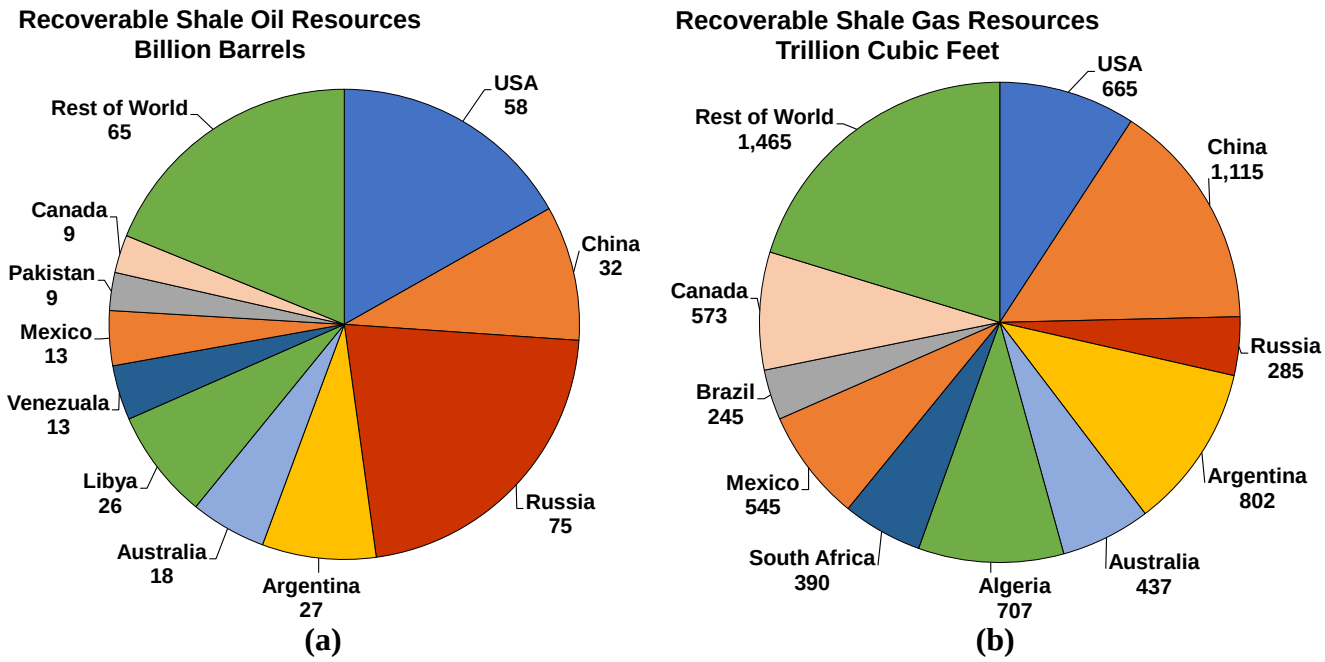

Figure 2: Map of basins with assessed shale and oil gas formations, May 2013 [1]

The largest shale deposits in the US are located in the Northeast, as shown in Figure 3, with the Utica and Marcellus shale plays producing most of the gas over the past decade. Shale sedimentary rocks have been long known as a source and reservoir of natural gas. They are formations associated with the deposition of thin-grained minerals and organic matter at the bottom of ancient seas, exposed to high pressure and temperature, where shale rocks containing light hydrocarbon deposits, primarily methane (~ 90%), are formed [2, 3]. Compared to conventional oil and gas deposits, which flow freely through rock formations, shale gas and oil do not flow naturally. This is because shale as a sedimentary reservoir rock has near-zero permeability (i.e., impermeable) for fluids to flow through it, and therefore it has to be fractured to enable the hydrocarbons to flow towards the production wells.

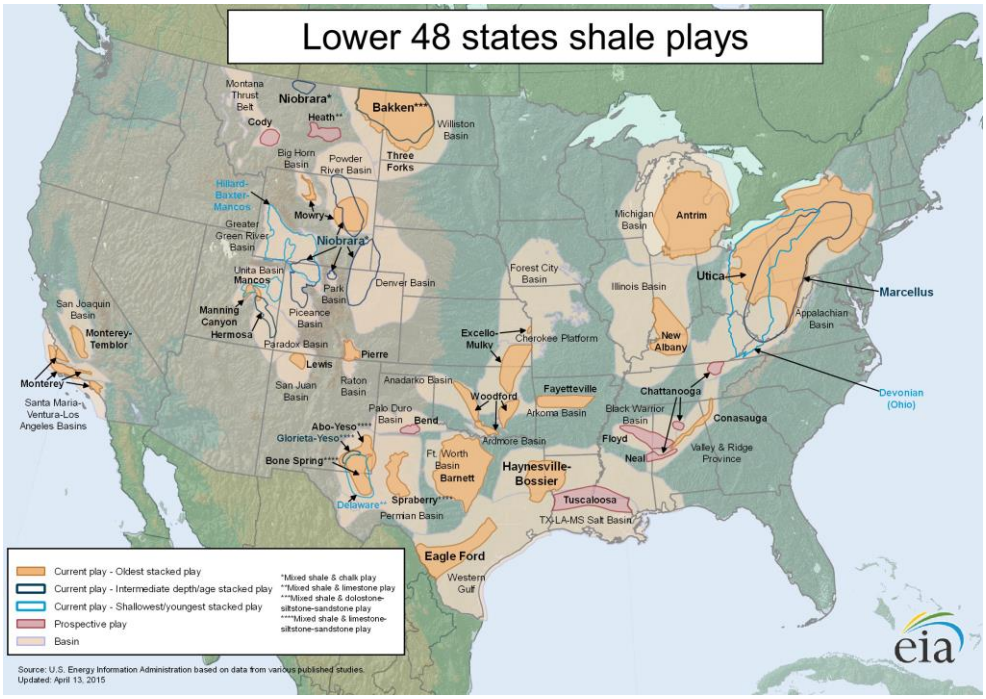

Figure 3: Shale gas plays in the USA [1]

Hence, with only the advances in horizontal drilling and hydraulic fracturing technologies that shale gas turned out to be profitably recoverable [2]. Horizontal drilling increases the areal contact between the well and the formation, thus enhancing the amount of gas to be recovered. Also, hydraulic fracturing is employed to create fractures, allowing the gas to flow through the fractured shale towards the wellbore. As a result, the combination of those techniques allowed an exponential rise in the shale gas production in the US since the mid-2000's, as can be observed in Figure 4 [3]. Table 1 compares the geological and production data for different shale gas formations in the US.

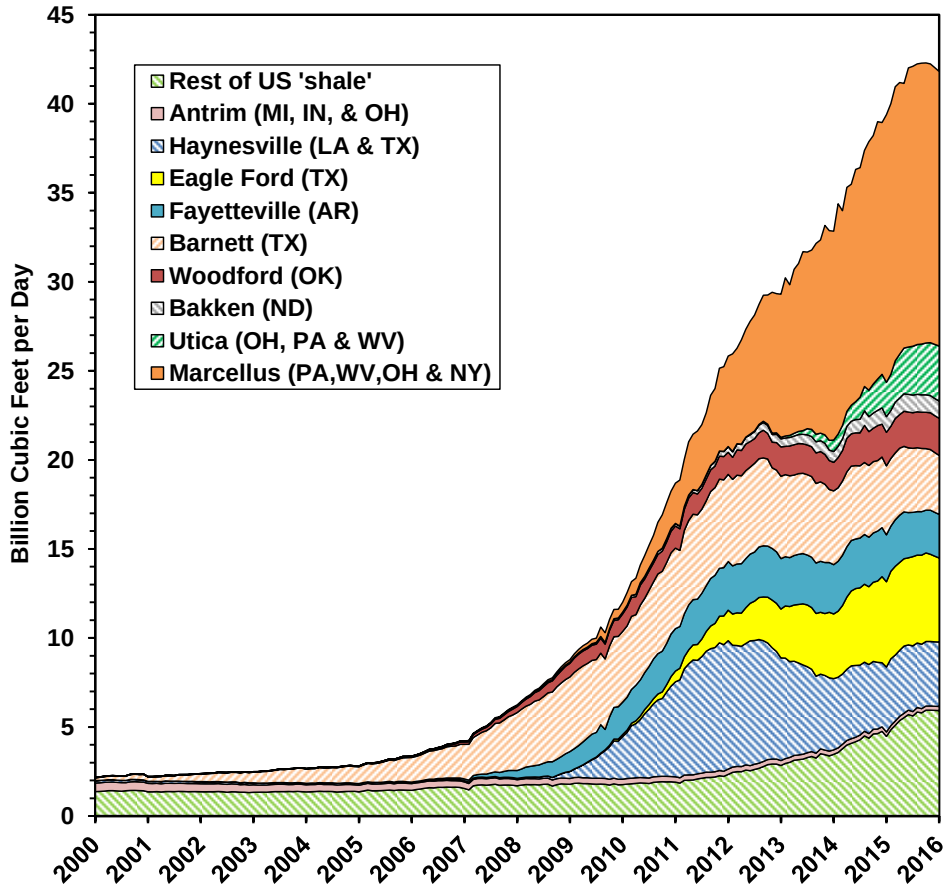

Figure 4: Shale gas production from different shale plays in the US

Table 1: Characteristics of the major US shale gas plays [4, 5].

Shale Basin	Barnett	Fayetteville	Haynesville	Marcellus	Woodford	Antrim	New Albany
Area (sq. miles)	5,000	9,000	9,000	95,000	11,000	12,000	43,500
Depth (ft)	6,500 – 8,500	1,000 – 7,000	10,500 – 13,500	4,000 – 8,500	6,000 - 11,000	600 – 2,200	5000 - 2000
Thickness (ft)	100 – 600	20 - 200	200 - 300	50 - 200	120 - 220	70 - 120	50 - 100
Depth to base of treatable water (ft)	1,200	500	400	850	400	300	400
Rock column between pay and base of treatable water	5,300 – 7,300	500 – 6,500	10,100 – 13,100	2,125 - 7,650	5,600 – 10,600	300 – 1,900	100 – 1,600
Total organic carbon (%)	4.5	4 – 9.8	0.5 – 4	3 – 12	1 – 14	1 – 20	1 – 25
Total porosity (%)	4 – 5	2 – 8	8 – 9	10	3 – 9	9	10 – 14
Gas content (scf/ton)	300 – 350	60 – 220	100 – 330	60 – 100	200 – 300	40 – 100	40 – 80
Water production (Barrels/day)	0	0	0	0	-	5 – 500	5 – 500
Well spacing (Acres)	60 – 160	80 – 160	40 – 560	40 - 160	640	40 – 160	80
Original Gas-in-Place (tcf)	327	52	717	1,500	52	76	160
Reserves	44	42	251	363 – 500	11.4	20	19.2
Estimated production (mcf/day/well)	338	530	625 – 1800	3,100	415	125 – 200	-

During hydraulic fracturing, millions of cubic meters of fracturing fluid, which is a mixture of water, chemicals and proppant are pumped into the wellbore at a flow rate high enough to increase the pressure at the target depth to exceed that of the fracture in the rock in order to create multiple fractures [3]. Once the fracture is formed, the fracturing fluid with the proppant infiltrates the rock, thus extending the fracture. Depending on its distance from the well, a fracture starts to localize as the pressure drops off. Typically, operators try to control the fracture width and slow its closure by adding proppants to the injected fluid, which are granular materials, such as sand, ceramic, or other solid particulates, which prevent the fractures from closure once the injection is stopped. As such, the propped fractures become permeable to allow the gas, oil, and water to the flow through the formation toward the wellbore [3, 4].

Figure 5 shows an overview of a typical hydraulic fracturing process. It was estimated that between 7,000 m^3 and 18,000 m^3 of water is used per well. Also, it was estimated that > 90% of hydraulic fracturing fluid is water and the remaining (< 10%) is a complex mixture of chemicals and proppant used to initiate and improve the fracture performance. The composition of the chemicals used depends on the nature of the rock formation [2, 4]. Despite being less than 1%, these chemicals cannot be ignored when considering the huge volume of the fluid injected. Often, these chemicals are proprietary and their compositions are unknown, which has become an area of public concern and mistrust of the hydraulic fracturing operation.

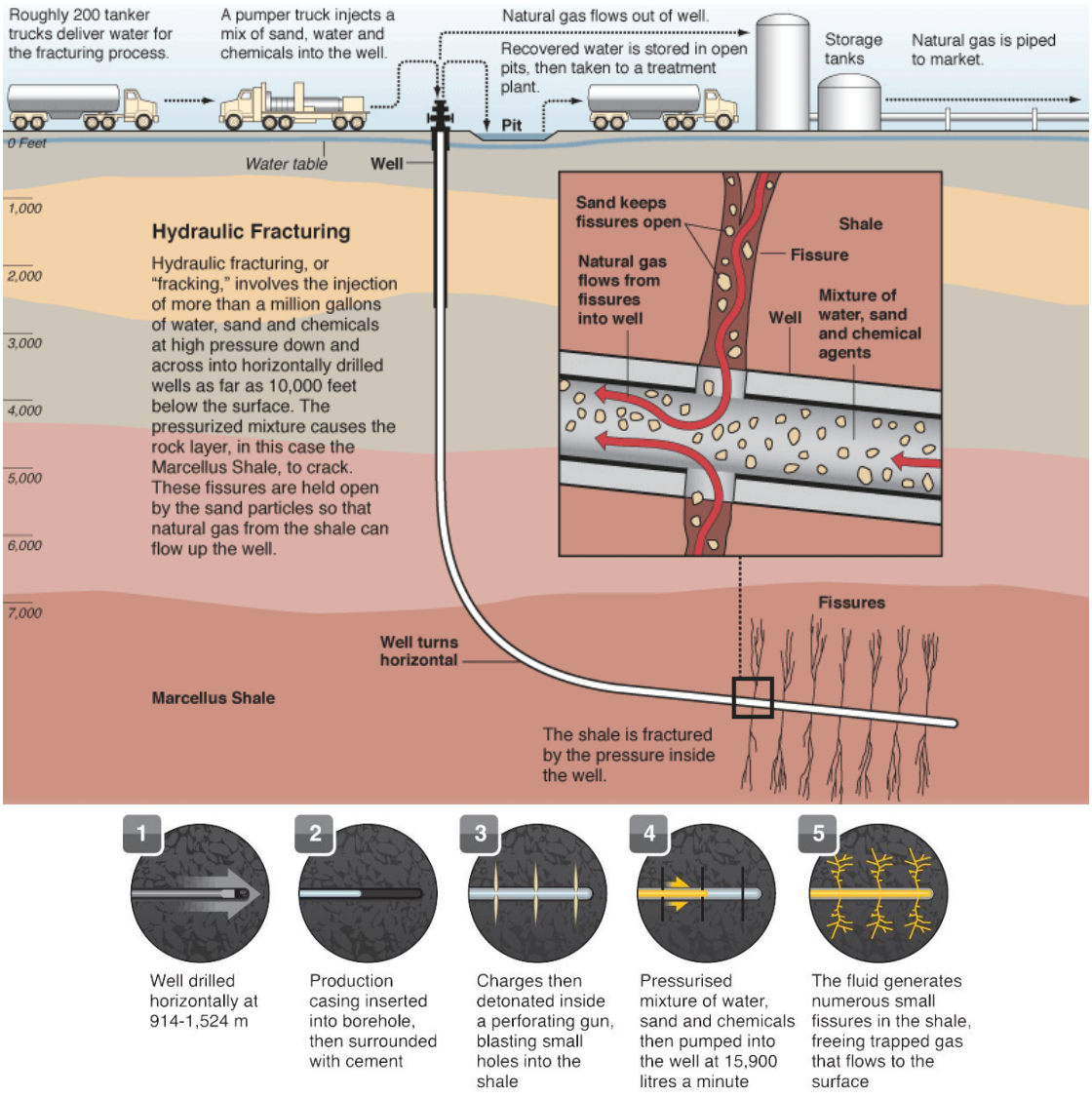

Figure 5: Overview of hydraulic fracturing process [6, 7]

Another area of concern is the immediate water that flows back to the wellhead after the hydraulic fracturing operation is completed, called flowback water, in addition to the water associated with the gas produced after the well is put on stream, known as produced water. It is estimated that 10% to 40% of the injected fracturing fluid returns to the surface as flowback water [2, 8]. This flowback water is produced over a period of about 2 weeks and is the largest amount of wastewater, which has to be dealt with in the hydraulic fracturing operation [2]. The flowback water often contains

high percentage of the total dissolve solids (TDS), typically about 10,000 to 300,000 mg/liter [2], and includes some fracking chemicals, minerals, organic compounds and even radionuclides [9]. The presence of the TDS is a result of the hydraulic fracturing fluids interaction with the shale rock formation in the reservoir.

There are several options to manage the flowback water produced as a result of shale gas hydraulic fracturing. The key methods include (1) on-site treatment of the flowback water for reuse in hydraulic fracturing of other wells, (2) use of publicly owned treatment works (POTW), (3) processing in industrial water treatment plants, and (4) disposal in deep reservoirs.

There has been an increased drive for more environmentally responsible management of flowback water produced as a result of fracturing operations. This can be demonstrated by the increasing trend of water reuse in Marcellus shale, and the increasing use of industrial and POTW treatment plants [10, 11]. Nonetheless, there remain significant challenges in the management of backflow water, primarily with regards to how to efficiently and economically treat this water before reuse in order to meet the increasingly stringent environmental guidelines.

2.0 BACKGROUND

2.1 ROLE OF WATER IN HYDRAULIC FRACTURING

The fracturing fluid consists mainly of water, multiple proprietary chemicals and a proppant, such as sand, ceramic, or other solid particulates. In the fracking operation, it was estimated that huge volumes of water (7,000-18,000 m^3) and chemicals (800-2,000 m^3) are used per well [2]. The hydraulic fracturing water cycle consists of five main stages [4, 6]: (1) water acquisition, (2) chemicals mixing, (3) well design, (4) flowback and produced water, and (5) flowback water treatment and/or disposal. These stages, shown in Figure 6, are discussed in the following section.

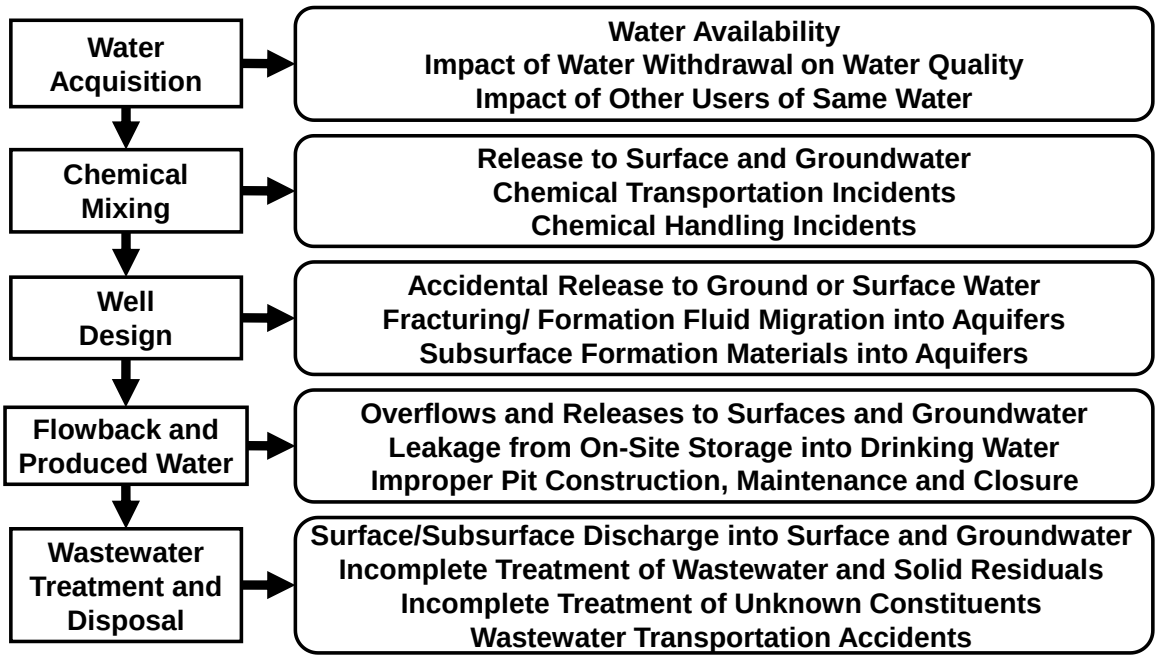

Figure 6: Summary of Technical, Logistical and Regulatory Considerations

2.2 WATER ACQUISITION

Hydraulic fracturing fluids contains approximately 90% water. Water demands per well's lifetime are estimated to be in the range of 50,000 m^3 for shale gas production, depending on the formation properties, well design and fracturing operation [12, 13]. This huge amount of water is typically sourced from groundwater, surface water or treated wastewater. The demand for water required for fracking activities raises concerns over the water availability, competition for drinking and irrigation purposes and its lifecycle [4, 13, 14]. Over the past decade, however, there has been an industrial trend to using treated and recycled produced water as a base fluid for hydraulic fracturing operations.

2.3 CHEMICAL MIXING

Chemicals are mixed with water to create the fracturing fluid to be pumped down the well. This fracturing fluid carries the proppant to the fracture and creates the required pressure needed to initiate and propagate the fractures into the bedrock. During the mixing process, chemicals are added to alter the fluid properties, such as pH, viscosity, surface tension, density etc., in order to optimize the performance of the fracturing operation. Most of these chemicals and proppants are preparatory and account for up to 10% of the hydraulic fracturing fluids. Figure 7 shows the composition of an available fracturing fluid and the percentages of each chemical component in the fluid [3, 4, 14].

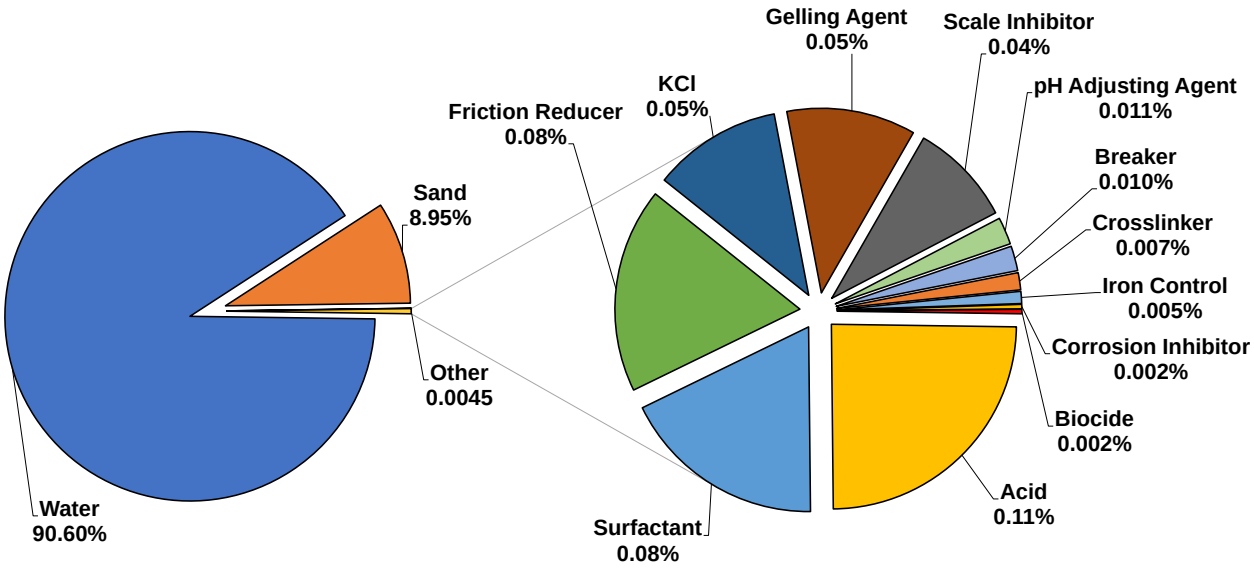

Figure 7: Fracturing fluid composition [4, 15]

2.4 WELL DESIGN

This step involves pumping the hydraulic fracturing fluid down the wellbore at pressures high enough to fracture the gas or oil bearing formation. This is typically carried out in shale formations with horizontal or vertical well completions. The production wells are drilled and completed in order to effectively produce the hydrocarbon from the reservoirs. These wells may be drilled and completed vertically, horizontally or directional wells [16].

2.5 FLOWBACK AND PRODUCED WATER

By the time the pressure applied to create the fracturing fluid through the shale rock is released, 10 to 40% of the fracturing fluid, now including formation water, organics and high concentrations of total dissolved solids (TDS), will flow back to the wellhead as a flowback water. In the first day, the rate of flowback may be as high as 1,000 m^3/day and then gradually decreases over a period of two weeks [2]. After the flowback water period, the well could continue to produces water associated with the gas at lower rates (2-8 m^3/day) throughout its lifetime, known as produced water [3, 9, 14, 17, 18].

The chemical properties of the flowback water are dependent on the type and location of the geological layers and the period of time that the injected fluid stays in contact with the formation. Flowback water constituents are essentially dissolved solid and hydrocarbons, which were present in the formation, and the chemicals added to the fracturing fluid as shown in Figure 7. In addition, flowback water may contain radionuclides and other unknown chemicals generated by the reactions between the injected fluid and the rock formation [2, 8, 14, 18]. Table 2 shows the chemical compositions and Table 3 shows the water quality from five different field studies to characterize flowback water chemistry in the Marcellus Shale [2, 19-22]. As shown in these tables, the TDS may reach concentrations as high as 345,000 mg/L, which is a major concern in water management. For instance, there are numerous risks related, not only to leakage, but also, to the challenges imposed by the high TDS in the water treatment, reuse and disposal [8]. Furthermore, the concentrations of barium, strontium, bromide and radioactive materials should be a matter of health and environmental concern due to the complexity related to their treatment.

Table 2: Chemical constituent ranges of Marcellus Shale flowback water [2, 19-22].

Chemical	Units	Minimum (average)	Maximum (average)
Alkalinity ($CaCO_3$)	mg/L	7.5	1100
Amenable Cyanide	mg/L	0.01	0.032
Ammonia Nitrogen	mg/L	29.4	199
Barium total	mg/L	0.24	13800
Bromides total	mg/L	0.2	1990
Calcium total	mg/L	37.8	41000
Chloride (Cl^-)	mg/L	64.2	196000
Cyanide total	mg/L	0.01	0.072
Fluoride	mg/L	0.05	17.3
Hardness ($CaCO_3$)	mg/L	5100	91000
Iron total	mg/L	2.6	321
Magnesium Total	mg/L	17.3	2550
Manganese total	mg/L	3	7
Nitrate-Nitrite	mg/L	0.1	1.2
Nitrite as N	mg/L	1.12	29.3
Oil and grease	mg/L	4.6	802
Phosphorus total	mg/L	0.01	2.5
Ra(226)	pCi/L	2.75	9280
Ra(228)	pCi/L	0	1360
Recoverable Phenolic total	mg/L	0.01	0.31
Sodium (Na+)	mg/L	69.2	117000
Strontium total	mg/L	0.59	8460
Sulfate (SO_4^{2-})	mg/L	0	763
Sulfide total	mg/L	3	5.6
Sulfite	mg/L	2.5	38

Table 3: Water quality parameters ranges of Marcellus Shale flowback water [2, 19-22].

Water Quality Parameter	Units	Minimum (average)	Maximum (average)
Biochemical Oxygen Demand(BOD)	mg/L	37.1	1,950
Chemical Oxygen Demand(COD)	mg/L	195	36,600
Conductivity	µmhos	133,100	173,200
Dissolved Organic Carbon (DOC)	mg/L	30.7	501.000
Gross Alpha	pCi/L	37.7	9,551.000
Gross Beta	pCi/L	75.2	597,600
Langelier Saturation Index (LSI)	LSI	0.55	1.020
Methylene Blue Active Substances (MBAS)	mg/L	0.012	1.520
pH		5.1	8.420
Specific Conductance	µmhos/cm	79,500	470,000
Specific Gravity	g/ml	1.065	1.087
Total Dissolved Solids (TDS)	mg/L	680	345,000
Total Kjeldahl Nitrogen*	mg/L	38	204
Total Organic Carbon (TOC)	mg/L	1.2	1,530
Total Suspended Solids (TSS)	mg/L	4	7,600

*Total Kjeldahl nitrogen or TKN is the sum of organic nitrogen, ammonia (NH_3), and ammonium (NH_4^+) in the chemical analysis of water.

2.6 WASTEWATER TREATMENT AND DISPOSAL

Water management involves several issues, such as environmental regulations, technology availability and economic feasibility [19]. In the US, underground disposal to manage flowback water is the most common approach [4]. Disposal wells, however, are not accessible all over the US, and they are particularly scarce in the Marcellus Shale region [2]. Public Owned Water Treatment Works are not allowed to receive flowback water by law in many states due to its elevated salt concentration, TDS and toxic compounds [23]. In the Marcellus Shale region, where disposal well are rarely available, shale gas producers reuse approximately 90% of flowback water as fracturing fluid [23]. Even so, there is still a large volume of wastewater to be managed, due to the massive volume of flowback water produced. Furthermore, using flowback water as fracturing fluid requires treatment to adjust the water parameters to meet industry standards. Alternatively, many shale gas producers have chosen to place flowback water in impermeable fluid surface storages, from which the wastewater is collected to be treated by specialized water treatment companies. However, large areas are required and production costs as well as environmental risks are significantly high [6].

Therefore, there is an urgency to develop feasible processes which are capable of treating flowback water in order to streamline the process and minimize environmental risks, such as polluting of surface and ground water and soil; and to decrease the huge amount of fresh water needed in the hydraulic fracturing operations. From an economic perspective, better water management is mandatory for the shale gas industry to keep increasing production in order to ensure the future supply of natural gas.

The technologies currently used in wastewater treatment include, physical, chemical, electrochemical, and thermal processes as well as membrane filtrations. In order to choose the best

treatment technologies, parameters, such as flowback water flowrate, TDS, Total Suspended Solids (TSS), water quality standards mandated by regulation for disposal of wastewater, and capital and operating costs, have to be considered [2, 19, 24].

2.6.1 Current Water Treatment Trends

Table 4 show that in 2012, there were 92,843 oil and gas wells in Pennsylvania, 93% of which were producing from conventional formations, while the remaining 7% were producing form the Marcellus Shale formation [8, 25]. Actually, 90% of all gas production and 92% of condensate (C_2 - C_5) in Pennsylvania came from unconventional gas wells [8, 25].

Table 4: Production data for Pennsylvania [8, 25].

Type of Hydrocarbon	# Producing Wells	Volume of Produced Water Brought to Surface	Volume of Hydrocarbon Produced
Crude oil from conventional formations	86,670	150,221 bbl/year (flowback) 6,812,303 bbl/year (produced water)	2,286,004 bbl/year (oil) 162,523 bbl/year (condensate)
Natural gas from conventional formations		218,141 MMCF/year	
Crude oil from unconventional formations	6,173	9,719,945 bbl/year (flowback) 17,406,287 bbl/year (produced water)	65,160 bbl/year (oil) 1,786,612 bbl/year (condensate)
Natural gas from unconventional formations		2,041,753 MMCF/year	
Total	92,843	34,088,756 bbl/year (based on volume of water managed)	4,300,299 bbl/year 2,259,894 MMCF/year

The Pennsylvania Department of Environmental Protection (PDEP) defines flowback water/fluid as: “the return flow of water, fracturing/stimulation fluids, and/or formation fluids recovered from the well bore of an oil or gas well within 30 days following the release of pressures induced as part

of the hydraulic fracture stimulation of a target geologic formation, or until the well is placed into production, whichever occurs first" [26]. Moreover, the PDEP defines Brine/Produced Fluids (comparable to produced water) as: "water and/or formation fluids, including natural salt water separated at oil and gas wells that are recovered at the wellhead after the flowback period" [26].

Table 5 provides a breakdown of the water management data in Pennsylvania during the unconventional drilling activities. As can be seen in this table, the highest utilization of flowback and produced waters is for reuse in activities other than road spreading (66.2%), which is not clear. However, this table shows an increasing trend for water reuse when compared with disposal.

Table 5: Water disposal methods in Pennsylvania (January to June 2015) [26].

Water Disposal Method	**Amount (BBL)**	**%**
Centralized waste treatment for discharge	1,362,225	6.5
Centralized treatment plant for recycle	83,618	0.399
Injection disposal well	1,798,364	8.59
Landfill	31,419	0.15
Residual waste processing facility (general permit)	3,662,234	17.5
Residual waste processing facility	22,343	0.107
Residual waste transfer facility	32,063	0.153
Reuse other than road spreading	13,863,624	66.26
Road spreading	147	0.0007
Storage pending disposal or reuse	65,739	0.314
Total	20,921,776	100

2.6.2 Water Quality Standards

Increasingly environmental regulations governing water quality standards have made it significantly difficult and expensive to treat water for reuse in a variety of applications. Table 6

provides a summary of the water quality parameters currently employed in the US. As can be observed in this table, there are numerous water quality parameters to take into consideration, such as pH, dissolved oxygen, alkalinity, chemical composition and radioactivity.

Table 6: Water Quality Parameter definitions and recommended limits [4, 15, 26-29].

Water Quality Parameter	Standard	Relevance
Specific conductance	–	A measure of the ability of water to conduct an electrical current; varies with temperature. Magnitude depends on concentration, kind, and degree of ionization of dissolved constituents; can be used to determine the approximate concentration of dissolved solids. Values are reported in microsiemens per centimeter at 25 °C.
pH	6.5-8.5 units SMCL	A measure of the hydrogen ion concentration; pH of 7.0 indicates a neutral solution, pH values smaller than 7.0 indicate acidity, pH values larger than 7.0 indicate alkalinity. Water generally becomes more corrosive with decreasing pH; however, excessively alkaline water also may be corrosive.
Temperature	–	Affects the usefulness of water for many purposes. Generally, users prefer water of uniformly low temperature. Temperature of groundwater tends to increase with increasing depth to the aquifer.
Dissolved oxygen	–	Required by higher forms of aquatic life for survival. Measurements of dissolved oxygen are used widely in evaluations of the bio- chemistry of streams and lakes. Oxygen is supplied to groundwater through recharge and by movement of air through unsaturated material above the water table.
Carbon dioxide	–	Important in reactions that control the pH of natural waters.
Hardness and non-carbonate hardness (as mg/L CaCO3)	–	Related to the soap-consuming characteristics of water; results in formation of scum when soap is added. May cause deposition of scale in boilers, water heaters, and pipes. Hardness contributed by calcium and magnesium, bicarbonate and carbonate mineral species in water is called carbonate hard- ness; hardness in excess of this concentration is called non-carbonate hardness. Water that has a hardness less than 61 mg/L is considered soft; 61-120 mg/L, moderately hard; 121-180 mg/L, hard; and more than 180 mg/L, very hard.
Alkalinity	–	A measure of the capacity of unfiltered water to neutralize acid. In almost all natural waters alkalinity is produced by the dis- solved carbon dioxide species, bicarbonate and carbonate. Typically expressed as mg/L CaCO3.
Dissolved solids	500 mg/L SMCL	The total of all dissolved mineral constituents, usually expressed in milligrams per liter. The concentration of dissolved solids may affect the taste of water. Water that contains more than 1,000 mg/L is unsuitable for many industrial uses. Some dissolved mineral matter is desirable, otherwise the water would have no taste. The dissolved solids concentration commonly is called the water's salinity and is classified as follows: fresh, 0-1,000 mg/L; slightly saline, 1,000-3,000 mg/L; moderately saline, 3,000-10,000 mg/L; very saline, 10,000-35,000 mg/L; and briny, more than 35,000 mg/L.
Calcium plus magnesium	–	Cause most of the hardness and scale-forming properties of water (see hardness).

Table 6 (continued)

Water Quality Parameter	Standard	Relevance
Sodium plus potassium		Large concentrations may limit use of water for irrigation and industrial use and, in combination with chloride, give water a salty taste. Abnormally large concentrations may indicate natural brines, industrial brines, or sewage.
Sodium- adsorption ratio (SAR)	–	A ratio used to express the relative activity of sodium ions in exchange reactions with soil. Important in irrigation water; the greater the SAR, the less suitable the water for irrigation.
Bicarbonate	–	In combination with calcium and magnesium forms carbonate hardness.
Sulfate	250 mg/L SMCL	Sulfates of calcium and magnesium form hard scale. Large concentrations of sulfate have a laxative effect on some people and, in combination with other ions, give water a bitter taste.
Chloride	250 mg/L SMCL	Large concentrations increase the corrosive- ness of water and, in combination with sodium, give water a salty taste.
Fluoride	4.0 mg/L MCL 2.0 mg/L SMCL	Reduces incidence of tooth decay when optimum fluoride concentrations present in water consumed by children during the period of tooth calcification. Potential health effects of long-term exposure to elevated fluoride concentrations include dental and skeletal fluorosis.
Nitrite (mg/L as N)	1.0 mg/L MCL	Commonly formed as an intermediate product in bacterially mediated nitrification and denitrification of ammonia and other organic nitrogen compounds. An acute health concern at certain levels of exposure. Nitrite typically occurs in water from fertilizers and is found in sewage and wastes from humans and farm animals. Concentrations greater than 1.0 mg/L, as nitrogen, may be injurious to pregnant women, children, and the elderly.
Nitrite plus nitrate (mg/L as N)	10 mg/L MCL	Concentrations greater than local back- ground levels may indicate pollution by feedlot runoff, sewage, or fertilizers. Concentrations greater than 10 mg/L, as nitrogen, may be injurious to pregnant women, children, and the elderly.
Ammonia	–	Plant nutrient that can cause unwanted algal blooms and excessive plant growth when present at elevated levels in water bodies. Sources include decomposition of animal and plant proteins, agricultural and urban runoff, and effluent from wastewater treatment plants.
Phosphorus, orthophosphate	–	Dense algal blooms or rapid plant growth can occur in waters rich in phosphorus. A limiting nutrient for eutrophication since it is typically in shortest supply. Sources are human and animal wastes and fertilizers.
Arsenic	10 µg/L MCL	No known necessary role in human or animal diet, but is toxic. A cumulative poison that is slowly excreted. Can cause nasal ulcers; damage to the kidneys, liver, and intestinal walls; and death. Recently suspected to be a carcinogen.

Table 6 (continued)

Water Quality Parameter	Standard	Relevance
Barium	2,000 µg/L MCL	Toxic; used in rat poison. In moderate to large concentrations can cause death; smaller concentrations can cause damage to the heart, blood vessels, and nerves.
Boron	–	Essential to plant growth, but may be toxic to crops when present in excessive concentrations in irrigation water. Sensitive plants show damage when irrigation water contains more than 670 µg/L and even tolerant plants may be damaged when boron exceeds 2,000 µg/L. The recommended limit is 750 µg/L for long-term irrigation on sensitive crops
Cadmium	5 µg/L MCL	A cumulative poison; very toxic. Not known to be either biologically essential or beneficial. Believed to promote renal arterial hypertension. Elevated concentrations may cause liver and kidney damage, or even anemia, retarded growth, and death.
Copper	1,300 µg/L (action level)	Essential to metabolism; copper deficiency in infants and young animals results in nutritional anemia. Large concentrations of copper are toxic and may cause liver damage. Moderate levels of copper (near the action level) can cause gastro-intestinal distress. If more than 10 percent of samples at the tap of a public water system exceed 1,300 µg/L, the US-EPA requires treatment to control corrosion of plumbing materials in the system.
Iron	300 µg/L SMCL*	Forms rust-colored sediment; stains laundry, utensils, and fixtures reddish brown. Objectionable for food and beverage processing. Can promote growth of certain kinds of bacteria that clog pipes and well openings.
Lead	15 µg/L (action level)	A cumulative poison; toxic in small concentrations. Can cause lethargy, loss of appetite, constipation, anemia, abdominal pain, gradual paralysis in the muscles, and death. If 1 in 10 samples of a public supply exceed 15 µg/L, the US-EPA recommends treatment to remove lead and monitoring of the water supply for lead content.
Lithium	–	Reported as probably beneficial in small concentrations (250-1,250 µg/L). Reportedly may help strengthen the cell wall and improve resistance to genetic damage and to disease. Lithium salts are used to treat certain types of psychosis.
Manganese	50 µg/L SMCL	Causes gray or black stains on porcelain, enamel, and fabrics. Can promote growth of certain kinds of bacteria that clog pipes and wells.
Mercury (inorganic)	2 µg/L MCL	No known essential or beneficial role in human or animal nutrition. Liquid metallic mercury and elemental mercury dissolved in water are comparatively nontoxic, but some mercury compounds, such as mercuric chloride and alkyl mercury, are very toxic. Elemental mercury is readily alkylated, particularly to methyl mercury, and concentrated by biological activity. Potential health effects of exposure to some mercury compounds in water include severe kidney and nervous system disorders

Table 6 (continued)

Water Quality Parameter	Standard	Relevance
Selenium	50 µg/L MCL	Essential to human and animal nutrition in minute concentrations, but even a moderate excess may be harmful or potentially toxic if ingested for a long time. Potential human health effects of exposure to elevated selenium concentrations include liver damage.
Radium-226 & 228 combined	5 pCi/L MCL	Radium locates primarily in bone; however, inhalation or ingestion may result in lung cancer. Radium-226 is a highly radioactive alkaline-earth metal that emits alpha- particle radiation. It is the longest lived of the four naturally occurring isotopes of radium and is a disintegration product of uranium-238. Concentrations of radium in most natural waters are usually less than 1.0 pCi/L.
Radon	300 or 4,000 pCi/L proposed MCL	Radium locates primarily in bone; however, inhalation or ingestion may result in lung cancer. Radium-226 is a highly radioactive alkaline-earth metal that emits alpha- particle radiation. It is the longest lived of the four naturally occurring isotopes of radium and is a disintegration product of uranium-238. Concentrations of radium in most natural waters are usually less than 1.0 pCi/L.
Strontium-90 (contributes to betaparticle and photon activity)	Gross beta-particle activity (4 millirem/ year)MCL	Strontium-90 is one of 12 un stable isotopes of strontium known to exist. It is a product of nuclear fallout and is known to cause adverse human health effects. Strontium-90 is a bone seeker and a relatively long-lived beta emitter with a half-life of 28 years. The USEPA has calculated that an average annual concentration of 8 pCi/L will produce a total body or organ dose of 4 millirem/year (U.S. EPA, 1997).
Thorium-230 (contributes to gross alpha-particle activity)	15 pCi/L MCL	Thorium-230 is a product of natural radio- active decay when uranium-234 emits alphaparticle radiation. Thorium-230 also is a radiological hazard because it is part of the uranium-238 decay series and emits alpha-particle radiation through its own natural decay to become radium-226. The half-life of thorium-230 is about 80,000 years.
Tritium (^{3}H) (contributes to betaparticle and photon activity)	Gross betaparticle activity (4 millirem/year) MCL	Tritium occurs naturally in small amounts in the atmosphere, but largely is the product of nuclear weapons testing. Tritium can be incorporated into water molecules that reach the Earth's surface as precipitation. Tritium emits low energy beta particles and is relatively short-lived with a half-life of about 12.4 years. The US-EPA has calculated that a concentration of 20,000 pCi/L will produce a total body or organ dose of 4 millirem/year.
Uranium	30 µg/L	Uranium is a chemical and radiological hazard and carcinogen. It emits alpha- particle radiation through natural decay. It is a hard, heavy, malleable metal that can be present in several oxidation states. Generally, the more oxidized states are more soluble. Uranium-238 and uranium-235, which occur naturally, account for most of the radioactivity in water. Uranium concentrations range between 0.1 and 10 µg/L in most natural waters.

* SMCL is secondary maximum contaminant levels

2.6.3 Water Treatment Methods

Figure 8 shows different water treatment technologies and their application to produced water, where the selection of any of these technologies is mainly controlled by its economics. For instance, if the cost/benefit ratio is too high, it becomes less appealing for drilling companies to treat the water produced. Table 7 summarizes the most common water treatment technologies with a scale-up potential for flowback water treatment. Among these technologies, reverse osmosis and nanofiltration, are the most promising ones due to their wide deployment in oil and gas industries. It is important to mention that technologies applicable for the treatment of produced water might be used in the treatment of flowback water due to their similar properties. The high TDS content of the flowback water, however, is a great challenge, requiring a thorough investigation before selecting the appropriate technology [30].

Treatment Method	De-Oiling	Suspended Solids Removal	Iron Removal	Ca & Mg Removal Softening	Soluble Organic Removal	Trace Organic Removal	Desalination & Brine Volume	SAR Adjustment	Silicate & Boron Removal
API Separator									
Deep Bed Filter									
Hydrocyclone									
Induced Gas Flotation									
Ultra-filtration									
Sand filtration									
Aeration & Sedimentation									
Precipitation Softening									
Ion Exchange									
Biological Treatment									
Activated Carbon									
Reverse Osmosis									
Distillation									
Freeze Thaw Evaporation									
Electrodialysis									
Chemical Addition									

Figure 8: Water treatment technologies and their application to produced water [31]

Table 7: Overview of the most common water treatment technologies.

Technology	Description	Industrial Status	Advantages	Disadvantages
Reverse Osmosis [32]	Membrane process which separates contaminants from an aqueous solution by applying pressure greater than the osmotic pressure to force water through a semipermeable membrane.	Main water desalination technology in the US. Processing more than 800 Million gal/d at 2,000 plants.	• Good track record with sea-water and brackish water. • Small footprint. • Handles a wide range of TDS concentrations • Organics and salts are removed	• Membrane fouling • Oil film on the membrane • Abrasion of membrane due to precipitates. • Poor water recoveries < 65%
Nanofiltration and Microfiltration [33]	Membrane process capable of retaining solutes as small as 1000 Daltons while passing solvent and smaller solutes. Surfactant addition enhances oil removal. Operating pressures of 140-410 kPa (20-60 psi) are far lower than reverse osmosis pressures.	Widely practiced on a large scale in industry. Micelle- enhanced version of this process is an emerging technology.	• Compact. • Removes 85-99% of total oil. • Effluent oil & grease can be reduced to below 14 ppm.	• Iron fouling can be a problem. • Effective cleaning is critical to prevent membrane fouling
Vapor Compression Distillation [34]	The process includes a multiple-effect evaporator that uses a compressor to pull a vacuum on the vessel that induces the boiling of water at low temperatures of 40º to 60º C. The heat for evaporating the water comes from the compression of vapor rather than the direct exchange of heat from steam produced in a boiler.	Commercially available at capacities of 120 to 120,000 bbl/d. Not yet adapted for produced water.	• High water recoveries of up to 98% can be achieved, even with concentrated feeds • Minimal fouling, scaling or plugging problems anticipated using the seeded slurry variant of VC	• Energy intensive compared to RO • Volatile organic contaminants follow the product water
Freeze Thaw Evaporation [35]	Freeze crystallization and thawing cycles are used to concentrate salts into a reduced volume of brine with the concomitant production of demineralized water. Evaporation is used to further reduce brine volumes in the summer.	Commercial deployment is in its first decade. Performance data from two commercial-scale FTE facilities is available.	• Low power requirements. • Can often be retrofitted to existing evaporation facilities.	• Only applies to areas that exhibit the required number of freeze days. • Land and labor required is significant.
Electro-dialysis[36]	In this process, ions are transferred through ion-selective membranes by means of a dc voltage. Cation-exchange membranes are alternated with anion exchange membranes in stacks.	Commercially available since the 1960's and employed in a number of industries including food, chemicals, and pharmaceuticals. Not commercially used in oil and gas industry.	• High water recoveries of > 92%. • Lower pressure operation (< 25 psi). • Resistant to fouling.	• Energy costs excessive at TDS > 15,000 mg/l • Does not remove BTEX or PAH's like naphthalene.

2.7 MEMBRANE FILTRATION

Membrane filtration is a widely applied technology for salt removal from produced water [30] and has also been extensively used for water desalination in the oil and gas industries. This technology is a physical transport phenomena designed to separate salt compounds in solution through concentration and pressure gradients. Table 8 shows the following classes of membranes used in the filtration process: (1) microfiltration, (2) ultrafiltration, (3) nanofiltration, and (4) reverse osmosis. In general, the membrane filters consist of films made of materials, such as polyamide, ceramics, polypropylene, polysulfone, cellulose acetate, and thin film composites. The filtration process can also be designed in different configurations, such as tubular, plate and frame, hollow-fiber and spiral-wound.

2.7.1 Microfiltration (MF) and Ultrafiltration (UF)

Microfiltration and ultrafiltration utilize membranes with pore sizes between 0.001-1.0 μm and are used to separate large molecules, such as clay, bacteria, viruses, protein, starch, colloidal silica, organics, dyes, fats, paint, and suspended solids.

Table 8: Different membrane filtration processes [30].

	Microfiltration	Ultrafiltration	Nanofiltration	Reverse Osmosis
Cut-off size	> 100 nm	10 - 100 nm	0.1 - 1 nm	< 0.1 nm
Filtered compound molecular weight	-	10^3 -10^5 kg/kmol	200 – 10^3 kg/kmol	< 10^3 kg/kmol
Transmembrane pressure	0.02 -0.5 MPa	0.2 - 1 MPa	0.5 -3 MPa	2 -20 MPa
Permeate flow	50 -1000 L/(m^2 h)	< 100 L/(m^2 h)	< 100 L/(m^2 h)	10 -35 L/(m^2 h)
Cross-flow speed	2 – 6 m/s	1 – 6 m/s	1 – 2 m/s	< 2 m/s
Retention mechanism	Screening by membrane pores	Screening by membrane and gel layer	Electrostatic repulsion and screening	Solubility and diffusion in the membrane
Transport mechanism	Hydrodynamic lift force	Back diffusion	Back diffusion	Back diffusion
Unit modules	Tubular, hollow-fiber	Tubular, hollow-fiber, spiral-wound, plate and frame	Tubular, hollow-fiber, spiral-wound, plate and frame	Tubular, hollow-fiber, spiral-wound, plate and frame
Materials retained	Clay, bacteria, viruses, suspended solids	Protein, starch, viruses, colloidal silica, organics, dyes, fats, paint, suspended solids	Starch, sugar, pesticides, herbicides, divalent anions, organics, BOD, COD, detergents	Metal cations, acids, aqueous salts, sugar, amino acids, monovalente salts, BOD, COD

2.7.2 Nanofiltration (NF)

Nanofiltration utilizes membranes with pore size between 0.1 and 1.0 nm, which permits to filter compounds with molecular weights between 200 and 1000 kg/kmol. To obtain such a small pore size, these membranes are composed of cellulose acetate or a thin film composite. Nanofiltration is operated under high pressure conditions between 0.50 and 3 MPa to allow flow through the membrane small pore sizes. The retention mechanism, however, is due to electrostatic repulsion and screening. Using either tubular, spiral, or plate and frame membrane configurations,

nanofiltration is often best used to filter starches, sugars, and biochemical oxygen demand (BOD) and chemical oxygen demand (COD). It should be noted that BOD and COD are two different means to measure how much oxygen is consumed by the water when it enters a recipient. For instance, if oxygen is consumed by water, this means that the water contains substances of an organic origin, which should be reduced to a minimum in the wastewater treatment plants. In general, industries are focusing on removing COD, whereas municipalities are focusing on removing BOD. In addition, nanofiltration has important commercial uses since it could remove pesticides, herbicides, and detergents.

2.7.3 Reverse Osmosis (RO)

Reverse osmosis utilizes membranes smaller than 0.1 nm. Because of such a small pore size, reverse osmosis membranes could handle compounds with a molecular weight in the range of 100-300 kg/kmol. As expected with such small pore sizes, reverse osmosis is typically operated under pressures ranging from 2 to 20 MPa. Reverse osmosis membranes are composed of cellulose acetate or a thin film composite containing polyamides. These membranes have a surface layer typically composed of polyamide, polysulfone on a polyester base. To handle high pressures, this dual layer is further reinforced by a fabric backing. Reverse osmosis is capable of handling sugars, BOD and COD. Actually, reverse osmosis is one of the most widely deployed water treatment technology due to its ability to filter metal cations, acids, aqueous and monovalent salts, in addition to amino acids. Therefore, the focus of this study is on nanofiltration and reverse osmosis technologies.

2.7.4 Commercial Membrane Configurations

Commercially available NF and RO membrane modules are tubular, plate and frame, spiral wound and hollow fiber. The difference among the membrane modules is how the membrane sheets are packed in order to increase the surface area per unit volume, thus making the unit more efficient and economic [37]. Spiral wound is the most common NF and RO membrane modules used at industrial-scale due to its high packing density, about 150-80 ft^2/ft^3. This means that a high flow rate is allowed in a considerably small filtration unit. In addition, the development of new membrane materials have enhanced the efficiency of these modules and decreased the operating costs by allowing high fluxes and enhanced solute rejection at low pressure [37, 38].

The spiral wound unit consists of leaves encompassed by two membrane sheets placed back to back, separated by a spacer and wound around a central perforated tube. Layers of membrane leaves are glued onto three sides, except on the side which is located around the perforated central tube, through which the permeate stream flows (Figure 9). The inlet flow of the system occurs through the feed spacer, then, normal to the inlet flow, water passes through the membrane sheets parallel to the spacer and is collected in the permeate spacer (also known as permeate carrier). The rejected solutes continue in the feed spacer stream, which becomes increasingly concentrated as contaminants are rejected. The filtered water in the permeate spacer goes towards the perforated central tube wherein the permeate streams gather to be collected and leave the unit. Also, the concentrate stream leaves the unit parallel to the permeate stream and both output leave the unit at the opposite side from which the feed water entered (Figure 10).

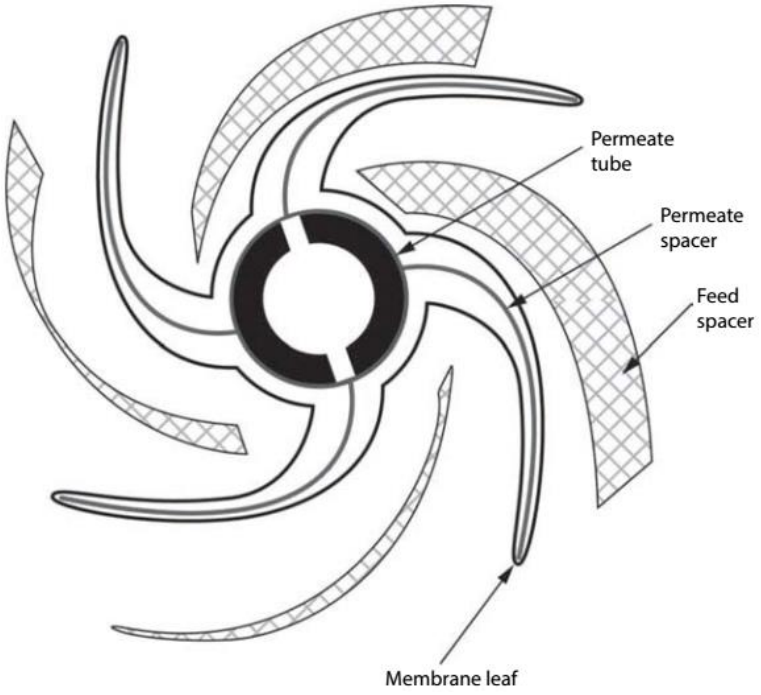

Figure 9: Spiral-would RO membrane module showing the different layers [37]

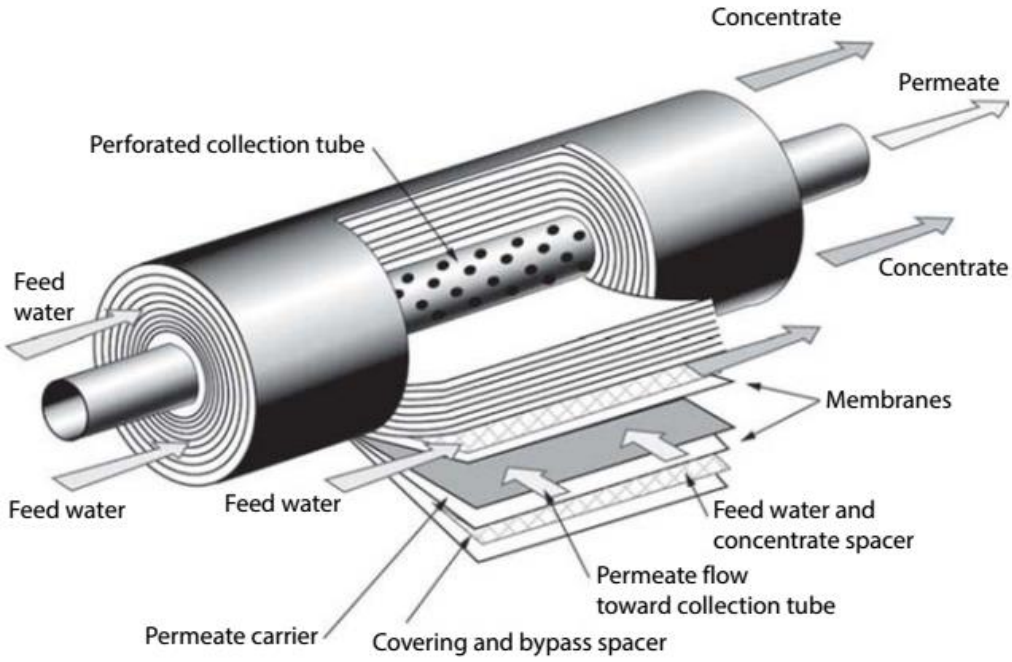

Figure 10: Typical configuration of spiral wound membrane [37]

3.0 OBJECTIVE

The main objective of this study is to assess through mathematical modeling the potential use and feasibility of deploying nanofiltration and reverse osmosis technologies in the treatment of flowback water produced during hydraulic fracturing operations. Field data of flowback water flow rate and chemical composition are used in the models in order to provide an accurate assessment of each technology. Operating conditions based on current commercial reverse osmosis and nanofiltration membranes for water treatment are also considered.

In order to achieve this objective the following tasks are completed:

Task 1: Two mathematical models, one for the reverse osmosis and one for the nanofiltration technologies, are developed and implemented in Matlab version R2015. Each model is based on the mass balance and thermodynamics in the respective membrane.

Task 2: A sensitivity analysis is conducted to determine the effect of operating variables on the membrane performance, and to evaluate the behavior of the key parameters for each technology.

Task 3: Four different reverse osmosis and three different nanofiltration commercial membranes, with varying materials, pore size and synthesis method, are used in this analysis.

4.0 RESEARCH APPROACH

In this section, the mathematical models are derived for the RO and NF processes and the operating parameters are defined. In the following section, the subscript (A) refers to the solvent (water), and the subscript (B) refers to the solute.

4.1 REVERSE OSMOSIS MODEL

The RO transport theory is explained through the Solution-Diffusion model proposed in 1995 by Wijmans and Baker [39]. This model states that the particles that permeate the membrane will dissolve before diffusing through it, following the gradient of their chemical potential. Thermodynamically, the pressure, temperature, concentration and other forces present in a given system are interrelated. The assumptions of the Solution-Diffusion model are:

(1) The fluids on each side of the membrane are in equilibrium, and hence there is a continuous chemical potential gradient from one side of the membrane to the other;

(2) At high pressures, which is intrinsic to the RO process, the pressure within the membrane is constant, and thus the chemical potential gradient across the membrane can be expressed only in terms of a concentration gradient; and

(3) The fluid and membrane are incompressible, and so the pressure profile is uniform within the membrane.

Figure 11 shows the chemical potential, pressure and solvent activity profiles of water across the membrane for the solution-diffusion model when applied to the reverse osmosis process.

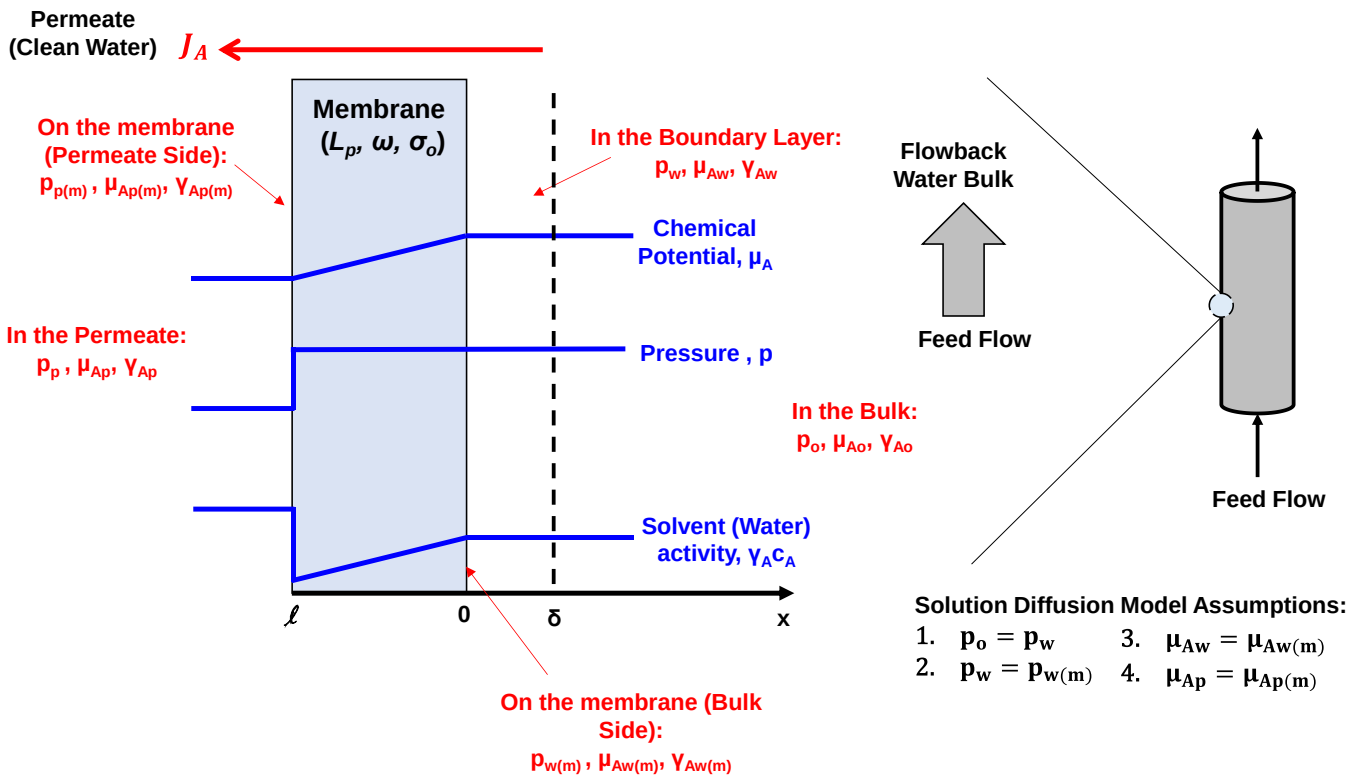

Figure 11: Chemical potential, pressure and solvent activity profiles

When water permeates the membrane due to the gradient of its chemical potentials, the flux through the membranes can be expressed as:

$$J_A = -L_i \left(\frac{d\mu_A}{dx}\right) \tag{1}$$

Where $(\frac{d\mu_A}{dx})$ is the gradient of the chemical potential; and L_i is a coefficient of proportionality (not necessarily a constant) linking the chemical potential driving force to the flux.

The change of the chemical potential can be written as:

$$d\mu_A = RTdln\,(\gamma_A c_A) + \nu_A dp \tag{2}$$

Where c_A, γ_A and ν_A are the concentration, activity coefficient and the molar volume of water; and p is the pressure.

Integrating Equation (2), leads to the chemical potential equation:

$$\mu_A = \mu_A^o + RTln(\gamma_A c_A) + \nu_A(p - p_A^o) \tag{3}$$

Where μ_A^o is the chemical potential of a pure water at a reference pressure, p_i^o.

Upon substituting the chemical potential term in Equation (2) as a function of concentration gradient at constant pressure, into Equation (1), the following expression for the diffusion term is obtained:

$$J_A = \frac{D_A\left(c_{Aw(m)} - c_{Ap(m)}\right)}{l} \tag{4}$$

Where D_A stands for the diffusion coefficient.

Therefore, from the initial assumption that the chemical potential of the water on the bulk and the permeate sides are in equilibrium across the membrane, the chemical potential in the fluid and on the respective membrane sides can be equated, as shown in Equations (5) and (6).

$$\mu_{Aw} = \mu_{Aw(m)} \tag{5}$$

$$\mu_{Ap} = \mu_{Ap(m)} \tag{6}$$

Where the subscript w stands for the wall-side, p stands for the permeate-side and m refers to the membrane.

Substituting in Equation (3) at the membrane interfaces gives the following chemical potential balances:

$$RTln(\gamma_{Aw}c_{Aw}) + \nu_A(p_w - p_{Asat}) = RTln(\gamma_{Aw(m)}c_{Aw(m)}) + \nu_A(p_o - p_{Asat}) \quad (7)$$

$$RTln(\gamma_{Ap}c_{Ap}) + \nu_A(p_p - p_{Asat}) = RTln(\gamma_{Ap(m)}c_{Ap(m)}) + \nu_A(p_o - p_{Asat}) \quad (8)$$

It should be noted that $p_o = p_w$, as shown in Figure 11. Therefore, rearranging in terms of the concentration at the wall-side in the membrane phase ($c_{iw(m)}$) leads to:

According to the second assumption $p_w = p_o$. Rearranging Equation (7) gives:

$$c_{Aw(m)} = \left(\frac{\gamma_{Aw}}{\gamma_{Aw(m)}}\right)c_{Aw} \quad (9)$$

The ratio of activity coefficients ($\frac{\gamma_{Aw}}{\gamma_{Aw(m)}}$) is known as the sorption coefficient, or the distribution coefficient or the partition coefficient of water across the membrane (K_{Aw}) and therefore:

$$c_{Aw(m)} = K_{Aw}c_{Aw} \quad (10)$$

Where:

$$K_{Aw} = \left(\frac{\gamma_{Aw}}{\gamma_{Aw(m)}}\right) \quad (11)$$

Similarly, by rearranging in terms of the water concentration at the permeate-side ($c_{Ap(m)}$) in the membrane phase leads to:

$$c_{Ap(m)} = K_{Ap} c_{Ap} \cdot exp\left[\frac{-\nu_A(p_o - p_p)}{RT}\right] \tag{12}$$

Where:

$$K_{Ap} = \left(\frac{\gamma_{Ap}}{\gamma_{Ap(m)}}\right) \tag{13}$$

Substituting Equations (10) and (12) into Equation (4), and denoting the pressure across the membrane $(p_o - p_p)$ as ΔP, gives the following expression for the water flux across the membrane:

$$J_A = \frac{D_A}{l}\left[K_{Aw} c_{Aw} - K_{Ap} c_{Ap} \cdot exp\left(\frac{-\nu_A \Delta p}{RT}\right)\right] \tag{14}$$

Similarly, the following expression can be obtained for the solute flux across the membrane:

$$J_B = \frac{D_B}{l}\left[K_{Bw} c_{Bw} - K_{Bp} c_{Bp} \cdot exp\left(\frac{-\nu_B \Delta p}{RT}\right)\right] \tag{15}$$

When the hydrostatic pressure across the membrane equals the osmotic pressure across the membrane ($\Delta p = \Delta \pi$), there is no flux, thus:

$$J_A = \frac{D_A}{l}\left[K_{Aw} c_{Aw} - K_{Ap} c_{Ap}.exp\left(\frac{-\nu_A \Delta p}{RT}\right)\right]\Big|_{\Delta p = \Delta \pi} = 0 \tag{16}$$

Rearranging:

$$c_{Ap} = c_{Aw}\left(\frac{K_{Aw}}{K_{Ap}}\right) exp\left(\frac{\nu_A \Delta\pi}{RT}\right) \tag{17}$$

For a hydrostatic pressure greater than $\Delta\pi$, combining Equations (14) and (17) gives:

$$J_A = \frac{D_A K_{AW} c_{Aw}}{l}\left(1 - exp\left[\frac{-\nu_A(\Delta p - \Delta\pi)}{RT}\right]\right) \tag{18}$$

In this case, the quantity ($\frac{D_A K_{Aw}}{l}$) represents the water permeability, κ_A, and therefore:

$$J_A = \kappa_A c_{Aw}\left(1 - exp\left[\frac{-\nu_A(\Delta p - \Delta\pi)}{RT}\right]\right) \tag{19}$$

Where:

$$\kappa_A = \left(\frac{Mw_A D_A K_{Aw}}{l}\right) \tag{20}$$

Since the pressure term is negligible under normal conditions of reverse osmosis, the exponential term can be reduced to $\left(1 - \frac{\nu_A(\Delta p - \Delta\pi)}{RT}\right)$. Using this approximation, Equation (18) becomes:

$$J_A = \kappa_A \frac{\nu_A}{RT}(\Delta p - \Delta\pi) \tag{21}$$

Subsequently, the quantity $\left(\kappa_A \frac{\nu_A}{RT}\right)$ represents the adjusted water permeability κ_A'.

Therefore:

$$J_A = \kappa_A'(\Delta p - \Delta\pi) \tag{22}$$

For the solute, since the pressure term in Equation (14) is negligible, another approach is to make $(\frac{-\nu_i(\Delta p-\Delta\pi)}{RT})$ equal zero, thus:

$$J_B = \frac{D_B K_B}{l}\left(c_{Bw} - c_{Bp}\right) \tag{23}$$

Where K_B is the averaged partition coefficient across the membrane [39].

In this case, the quantity $\left(\frac{D_B K_B}{l}\right)$ is the solute permeability, κ_B, and therefore:

$$J_B = \kappa_B\left(c_{Bw} - c_{Bp}\right) \tag{24}$$

Where:

$$\kappa_B = \left(\frac{Mw_B D_B K_B}{l}\right) \tag{25}$$

The dimensionally consistent representation of the relationship between J_A and J_B is as follows:

$$J_B = \left[\frac{Mw_B \kappa_B\left(c_{Bw} - c_{Bp}\right)}{\kappa_A c_{Aw}\left(1 - exp\left[\frac{-\nu_A(\Delta p - \Delta\pi)}{RT}\right]\right)}\right] J_A \tag{26}$$

Subsequently, the solute flux, J_B, can be related to the solvent flux J_A, as follows:

$$J_B = \alpha J_A \tag{27}$$

Where:

$$\alpha = \frac{\kappa_B\left(c_{Bw} - c_{Bp}\right)}{\kappa_A c_{Aw}\left(1 - exp\left[\frac{-\nu_A(\Delta p - \Delta\pi)}{RT}\right]\right)} \tag{28}$$

Therefore, Equation (19), (24), (27) and (28) describe the two fluxes and how they are related.

4.1.1 RO System Configuration: Singles Pass

Single-pass reverse osmosis operations are usually represented as a plug-flow reactor, with the assumptions that the system is not well mixed. This is because there is no recirculations, and the flow rate, concentration and the mass transfer coefficient vary with time. Figure 12 shows a schematic of the different streams in the single-pass RO operation.

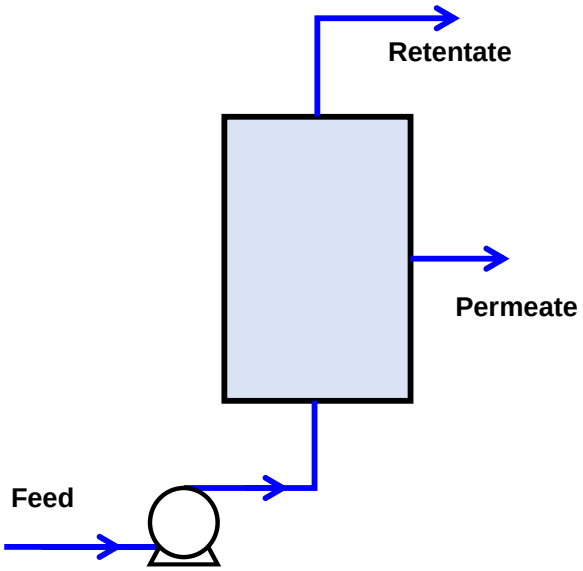

Figure 12: Single pass RO process

In order to derive a model to express the solution concentration in RO filtration in a single-pass system, the following two assumption were made:

(1) The pressure drop through the membrane is negligible, thus ΔP is constant.

Differentiating Equations (22), (24) and (26) at constant Δp gives:

$$dJ_A = -\kappa_A' \left(\frac{d\pi_{Aw}}{dc_{Aw}}\right) dc_{Aw} + \kappa_A' \left(\frac{d\pi_{Ap}}{dc_{Ap}}\right) dc_{Ap} \tag{29}$$

$$dJ_B = \kappa_B dc_{Bw} - \kappa_B dc_{Bp} \tag{30}$$

$$dJ_B = \alpha dJ_A + J_A d\alpha \tag{31}$$

Where π_{Aw} and π_{Ap} are the osmotic pressure expressed as functions of the concentrations at the wall (c_{Aw}) and permeate (c_{Ap}) side, respectively.

(2) At steady-state, the transport rate of particles into the membrane by convection and out of the membrane by diffusion are equal, as shown in Figure 13.

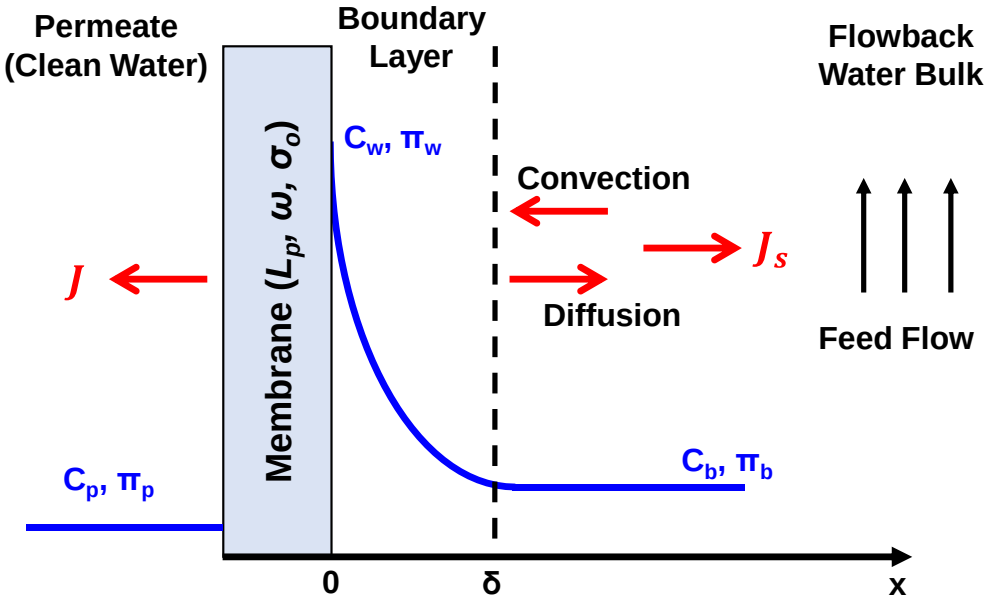

Figure 13: Concentration profile along the reverse osmosis membrane

Subsequently, the mass balance across the membrane can be represented as:

$$Jc_x - Jc_p - \left(-D\frac{dc_y}{dy}\right) = 0 \tag{32}$$

Assuming the diffusion coefficient (*D*) is constant and rearranging Equation (32) gives:

$$\frac{J}{D}\int_0^{\delta} dy = -\int_{c_w}^{c} \frac{dc_y}{(c_y - c_p)} \tag{33}$$

The integral limit on the left-hand-side from 0 to δ refers to an imaginary film, where the concentration gradient due to the concentration polarization phenomenon occurs. Hence, integrating and rearranging Equation (33) provides a different approach for the water flux across the membrane under the influence of the concentration polarization phenomenon.

$$J_A = \frac{D_A}{\delta}\ln\left(\frac{c_{Aw} - c_{Ap}}{c - c_{Ap}}\right) \tag{34}$$

The quantity $\left(\frac{D_A}{\delta}\right)$ represents the mass transfer coefficient, k_m, thus:

$$J_A = k_m ln\left(\frac{c_{Aw} - c_{Ap}}{c - c_{Ap}}\right) \tag{35}$$

By equating the expression for water flux derived from both the concentration polarization phenomenon, Equation (35), and the solution-diffusion model, Equation (19), provides the basic flux model:

$$k_m ln\left(\frac{c_{Aw} - c_{Ap}}{c - c_{Ap}}\right) - \kappa_A'(\Delta p - \Delta\pi) = 0 \tag{36}$$

Also, in order to obtain an expression for the concentration at the permeate side of the membrane (c_{Ap}), Equations (29), (30) and (31) were combined and divided by the differential area (dA), similar to the procedure of Foley [40] as:

$$\frac{dc_{Ap}}{dA} = \theta\left(\frac{dc_{Aw}}{dA}\right) \tag{37}$$

Where:

$$\theta = \frac{\kappa_B + c_{Ap}\kappa'_A\left(\frac{d\pi_A}{dc_{Aw}}\right)}{k_m \ln\left(\frac{c_{Aw} - c_{Ap}}{c - c_{Ap}}\right) + \kappa_B + c_{Ap}\kappa'_A\left(\frac{d\pi_{Ap}}{dc_{Ap}}\right)} \tag{38}$$

Differentiating and combining Equation (37) with Equations (36) and (38) gives:

$$\frac{dc_{Aw}}{dA} = \frac{\left(\frac{k_m}{c - c_{Ap}}\right)\frac{dc}{dA} - \ln\left(\frac{c_{Aw} - c_{Ap}}{c - c_{Ap}}\right)\frac{dk_m}{dA}}{\left(\frac{k_m\theta}{c - c_p}\right) + \frac{k_m(1-\theta)}{(c_{Aw} - c_{Ap})} + \kappa'_A\left(\frac{d\pi_{Aw}}{dc_{Aw}}\right) - \kappa'_A\theta\frac{d\pi_{Ap}}{dc_{Ap}}} \tag{39}$$

In order to study the dependence of the mass transfer coefficient on the flow rate, it was assumed that k is not a function of viscosity and consequently, it becomes only a function of the variation in the tangential flow rate, which is expressed as:

$$k_m = k_o\left(\frac{Q}{Q_o}\right)^n \tag{40}$$

Where k_o and Q_o are the mass transfer coefficient and the flow rate at the inlet conditions, respectively; and n is an empirical constant with values within the following inequalities $0 \leq n \leq 1$. For turbulent flow in single-pass systems; n is frequently = 0.8.

Differentiating Equation (40) and (31) provides:

$$\frac{dk_m}{dA} = \frac{nk_m}{Q}\frac{dQ}{dA} \tag{41}$$

Assuming that the Van't Hoff equation is applicable to the system gives:

$$\frac{d\pi_{Aw}}{dc_{Aw}} = \frac{d\pi_{Ap}}{dc_{Ap}} = IRT \tag{42}$$

Where *I* is the Van't Hoff factor, which is a measure of the effect of the solute on the osmotic pressure. The Van't Hoff factor is equal to 1 for non-electrolytes dissolved in water, and is equal to the number of discrete ions in the formula unit of dissolved ionic compounds [41].

From the mass balance, the change of the tangential flow rate (dQ) and bulk concentration (c) over a differential area (dA) can be expressed as:

$$\frac{dQ}{dA} = -J \tag{43}$$

$$c\frac{dQ}{dA} + Q\frac{dc}{dA} = -J_B \tag{44}$$

Substituting Equation (43) into Equation (44) gives:

$$\frac{dc}{dA} = \frac{1}{Q}(cJ - J_B) \tag{45}$$

Combining Equations (27) and (45) leads to:

$$\frac{dc}{dA} = \frac{J}{Q}\left(c - c_{Bp}\right) \tag{46}$$

Finally, substituting Equations (41), (42), (43) and (46) into Equation (39), a first order differential equation for the concentration on the membrane as a function of the differential channel (membrane) surface area is obtained as:

$$\frac{dc_{Bw}}{dA} = \frac{\frac{k_m J}{Q}\left[1 + n\left(ln\frac{c_{Aw} - c_{Ap}}{c - c_{Ap}}\right)\right]}{\frac{k\theta'}{c - c_{Bp}} + \frac{k_m(1-\theta')}{c_{Bw} - c_{Bp}} + \kappa_A' iRT - \kappa_A' iRT\theta'} \tag{47}$$

$$\frac{dc_{Bw}}{dA} = \frac{\frac{k_m}{c - c_p}\frac{dc}{dA} - \frac{nk_m}{Q}\left(ln\frac{c_{Aw} - c_{Ap}}{c - c_{Ap}}\right)\frac{dQ}{dA}}{\frac{k_m\theta'}{c - c_{Bp}} + \frac{k_m(1-\theta')}{c_{Bw} - c_{Bp}} + \kappa_A' iRT - \kappa_A' iRT\theta'} \tag{48}$$

Where θ' is:

$$\theta' = \frac{\kappa_B + c_{Ap}\kappa_A iRT}{k_m \ln\left(\frac{c_{Aw} - c_{Ap}}{c - c_{Ap}}\right) + \kappa_B + c_{Ap}\kappa_A' iRT} \tag{49}$$

4.2 NANOFILTRATION MODEL

Typically, the solute transport in the nanofiltration process is derived from non-equilibrium thermodynamics, based on the extended Nernst-Plank Equation, which accounts for three main driving forces, diffusion, electrical charge and convection [42-45]:

$$J_B = D_B\left(\frac{dc_B}{dx}\right) + J_{electrical} + (1-\sigma_o)J_A\frac{c_{Bav}}{v_A \times 10^3} \quad (50)$$

The the first term on the right-hand-side represents the flux due to diffusion, the second term represents the flux due to electrical charge and the third term represents the flux due to convection, and σ_o is the osmotic reflection coefficient. The flux due to electrical charge is usually insignificant, except in the case of charged membrane filtration or in electrolysis. The osmotic reflection coefficient (σ_o) is an inherent property of the membrane, which is representative of the convective flow. Thus, if the osmotic reflection coefficient approaches 1, the higher the solute rejection will be.

The main difference between nanofiltration and reverse osmosis filtration processes, however, lies in the fact that the convection term plays a significant role on the overall flux in the nanofiltration process. This is due to the fact that the large pores of the nanofiltration membranes result in more dominant convective forces in the vicinity of the membrane, as reported by several investigators theoretically [46-48] and experimentally [48-51].

Subsequently, the solute flux is represented as a function of the diffusive flux, which is derived in an identical manner to the reverse osmosis, and the convective flux, which depends on the osmotic reflection coefficient (σ_o) as follows:

$$J_B = \kappa_B\left(c_{Bw} - c_{Bp}\right) + (1-\sigma_o)J_A\frac{c_{Bav}}{v_A \times 10^3} \quad (51)$$

Where κ_B is the solute permeability in units of (m/s) and c_{Bav} is the average solute concentration in the membrane represented by the log-mean average:

$$c_{Bav} = \frac{c_{Bw} - c_{Bp}}{\ln\left(\frac{c_{Bw}}{c_{Bp}}\right)} \tag{52}$$

It should be mentioned, however, that the water or permeate flux (J_A) in nanofiltration process can be written using Equation (53), which is identical to (19) for the reverse osmosis process:

$$J_A = \kappa_A c_{Aw}\left(1 - exp\left[\frac{-v_A\left(\Delta p - \sigma_o RT\left(c_{Aw} - c_{Ap}\right)\right)}{RT}\right]\right) \tag{53}$$

Where:

$$\sigma_o RT\left(c_{Aw} - c_{Ap}\right) = \Delta\pi \tag{54}$$

The water permeability, $\kappa_{A,}$ is in units of (m/s), ΔP is the pressure drop across the membrane in Pa, and σ_o is the osmotic reflection coefficient.

For modeling the nanofiltration process, there are three unknowns: the bulk concentration (c), the permeate concentration (c_p), and the concentration at the wall (c_w), and therefore three equations are needed in order to solve for these unknown. The first one is Equation (27), which can be used to relate the flux equations expressed in Equations (22) and (24). The second one is Equation (36), which combines the concentration polarization phenomenon and the osmotic pressure [39, 40]. The third one is Equation (35), which describes the water mass transfer across the membrane.

4.2.1 Nanofiltration System Configuration: Fed-Batch

A fed-batch system configuration is assumed for the nanofiltration process, as shown in Figure 14, with a volume (V_o) with an initial solute concentration (c_o). The mass balance for this system with membrane area A is:

$$V_o \frac{dc}{dt} = A(-J_B + J_A) \tag{55}$$

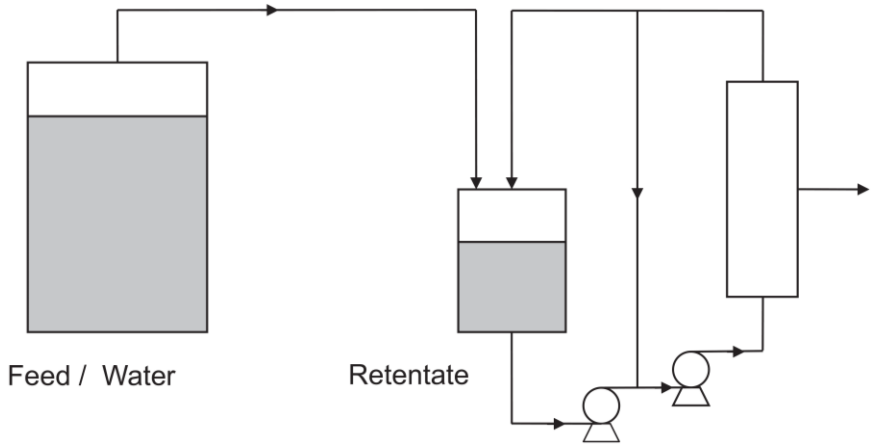

Figure 14: Batch-fed nanofiltration process (Taken from Foley [40])

With three equations, the system can be modeled for c, c_p, and c_w. Equations (27) and (35) are algebraic equations and Equation (55) is a differential equation. As a result, a 3x3 identity matrix was used to identify Equation (55) as the only differential equation to be solved. This produces the following system of equations to be solved by MATLAB:

$$\begin{pmatrix} 1 & 0 & 0 \\ 0 & 0 & 0 \\ 0 & 0 & 0 \end{pmatrix} \begin{pmatrix} dc/dt \\ dc_{Bw}/dt \\ dc_{Bp}/dt \end{pmatrix} = \begin{pmatrix} -(J_A A - JA)/V_0 \\ J_B - \alpha J_A \\ \ln\left(\frac{c_{Aw} - c_{Ap}}{c - c_{Ap}}\right) - \frac{J_A}{k_m} \end{pmatrix} \quad (56)$$

The identity matrix at a value of positive one indicates that this system of equations will model the concentration increase on the permeate side of the membrane.

4.3 OPERATING PARAMETERS

Table 9 shows the concentrations and mass transfer coefficients of the different chemical species in the flowback water used in this study [2]. Using the model developed by Voros et al. [52], the solute permeability for the ions Cl^-, Na^+ and Ca^{2+}, representing the highest ion concentrations in flowback water, were calculated as shown in Table 10. Moreover, four different RO membranes [53] and three different NF membranes [54] with the properties given in Tables 11 and 12, respectively, were used in the analysis. Also, the operating conditions used in this study are given in

Table **13**.

Table 9: Concentration and permeability of different chemical species in flowback water [2]

Solute		k (μm/s)	Concentration in Flowback water (mg/L)	Molar Mass (kg/kmol)
Chloride (Cl^-)	Cl	11.16	98032.1	35.453
Sodium (Na^+)	Na	17.24	58534.6	22.99
Calcium total	Ca	8.24	20518.9	40.078
Barium total	Ba	2.89	6900.12	137.328
Strontium total	Sr	4.52	4230.295	87.62
Magnesium Total	Mg	16.30	1283.65	24.305
Bromine total	Br	4.96	995.1	79.904
Potassium Total	K	10.14	281	39.098
Iron total	Fe	7.10	161.8	55.845
Ammonia Nitrogen	NH_3-N	12.78	114.2	17.031
Boron	B	36.65	20	10.811
Manganese total	Mn	7.21	5	54.938
Sulfide total	SO_4	4.08	4.3	96.062
Phosphorus total	P	12.79	1.255	30.974
Aluminum	Al	14.69	0.5	26.982
Zinc	Zn	6.06	0.09	65.38

Table 10: Solute permeability values calculated using Voros et al. model [52]

Species	Solute Permeability, k_A (m/s)
Cl^-	4.1×10^{-9}
Na^+	8.6×10^{-6}
Ca^{2+}	1.8×10^{-9}

Table 11: Water permeability for various commercial RO membranes [53]

RO Membrane	Selective Layer Material	Water Permeability, k_A (m/s)
XLE	Polyamide	2.06×10^{-11}
ESPA1	Polyamide	1.50×10^{-11}
BW30	Polyamide	8.33×10^{-12}
SWC4+	Polyamide	1.94×10^{-12}

Table 12: Water permeability for various commercial NF membranes [54]

NF Membrane	Selective Layer Material	Water Permeability, k_A (m/s)
TFC-SR (Koch)	Polyamide	5.47×10^{-11}
NF-70 (Dow)	Polypiperazine amide	7.22×10^{-12}
NF-90 (Dow)	Polypiperazine amide	1.00×10^{-11}

Table 13: Operating conditions used in this study

Parameters	Nomenclature	Unit	Min	Max	Average
Flowback flow rate – Inlet Flow rate	Q_o	m^3/s	5.0×10^{-4}	5.0×10^{-3}	2.75×10^{-3}
Operating Pressure	ΔP	MPa	5.5	20	12.75
Temperature	T	K	-	-	298.0
Gas Constant	R	$Pa.m^3/K/mol$	-	-	8314
Van't Hoff Coefficient	*i*	-	-	-	1.0
Module diameter [37]	D	m	-	-	0.2
Module length [37]	L	m	-	-	1.0
Module surface area [37]	A	m^2	-	-	41.0
Module permeate flow rate [17]		m^3/s	-	-	3.15×10^{-4}
Module packing density [37]		m^2/m^3	492	1247	869.5

5.0 RESULTS AND DISCUSSIONS

5.1 SENSITIVITY ANALYSIS FOR REVERSE OSMOSIS PARAMETERS

In the following section, a sensitivity analysis of the factors affecting the reverse osmosis process is conducted. It should be noted that the RO model is only a function of membrane surface area.

5.1.1 Effect of Water Permeability (κ_A)

Figure 15 shows the effect of water permeability change between 1.6 and 3.4 μm/s on the solute concentrations calculated using the RO model. As can be observed in this figure, as the water permeability increases, the rate of solute concentration decreases, which leads to low overall bulk concentration levels. Physically, this is achievable because if more water is allowed to pass through the membrane, the better the filtration results will be.

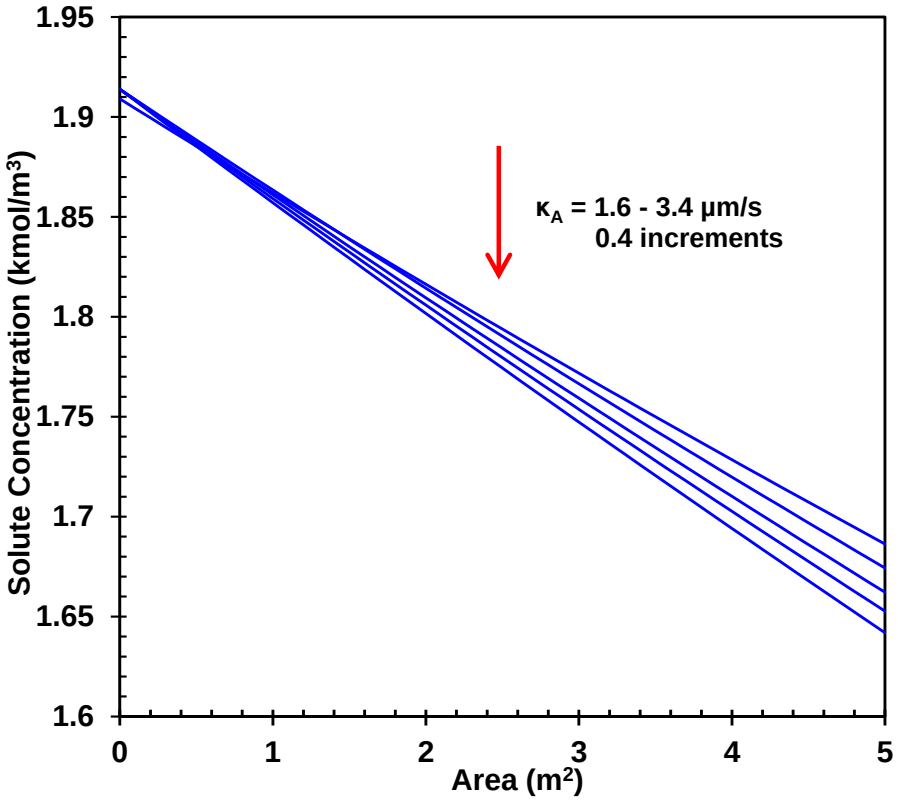

Figure 15: Effect of water permeability on the solute concentration for the RO model

5.1.2 Effect of Pressure Drop (ΔP)

Figure 16 shows the effect of the pressure drop across the membrane change from 1.5 10.5 MPa on the solute concentration and as can be seen, increasing the pressure drop decreases the bulk solute concentration. This was expected since high pressure drop should increase the water flux, leading to faster filtration per unit membrane area.

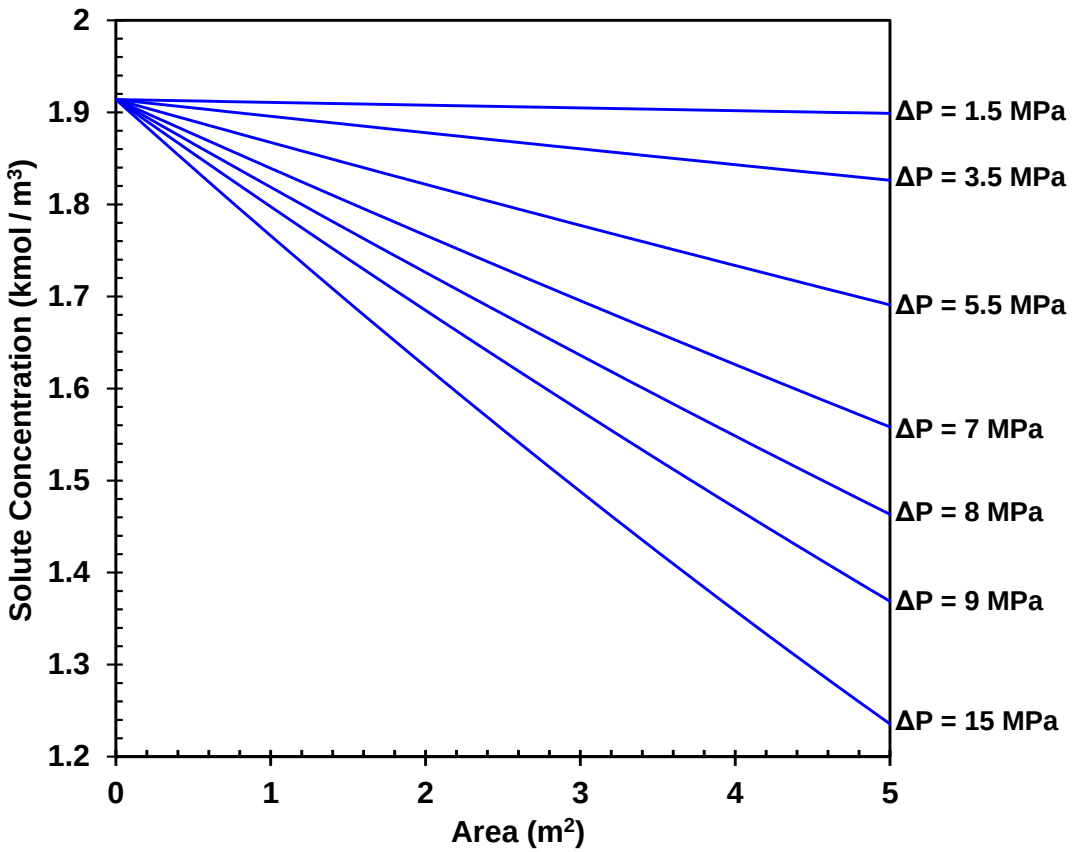

Figure 16: Effect of pressure drop on the solute concentration for the RO model

5.1.3 Effect of Temperature (T)

Figure 17 shows the effect of RO process temperature variation within the range 275-370 K on the solute concentration and as can be seen as temperature increases, the solute concentration decreases. This is primarily due to the effect of temperature on the osmotic pressure, as shown in Equation (42). As the temperature increases, it increases the osmotic pressure, which leads to the decrease of the water flux.

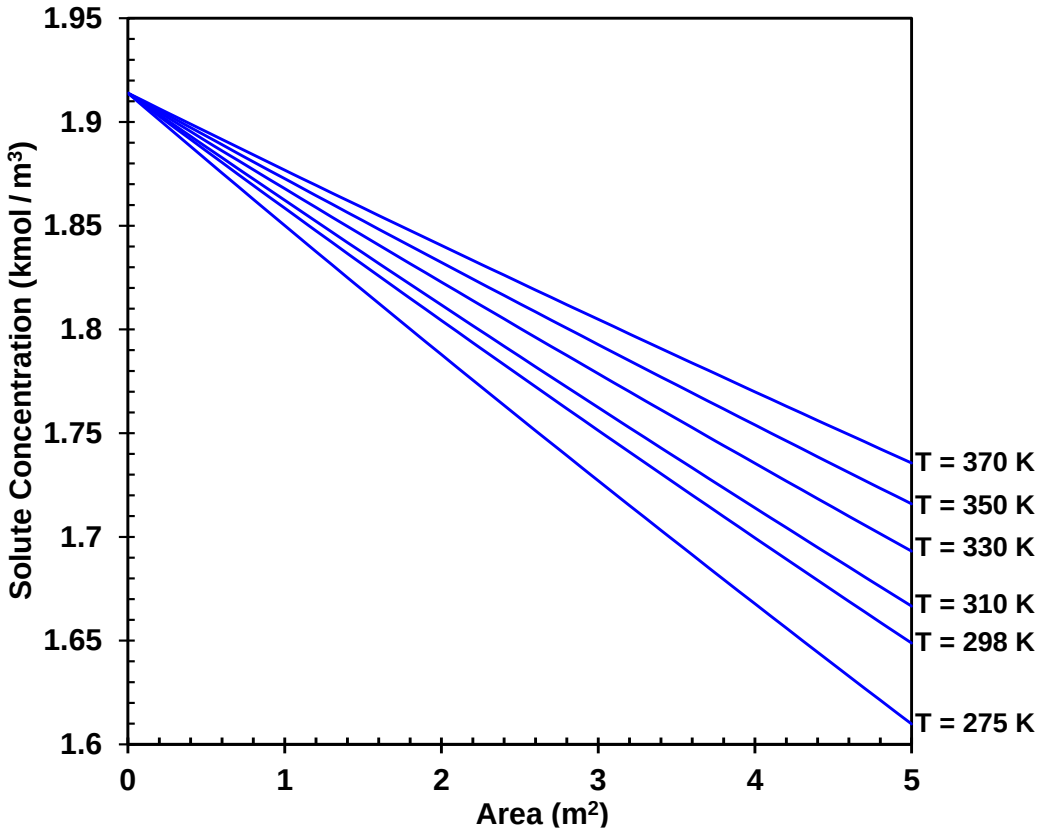

Figure 17: Effect of temperature on the solute concentration for the RO model

5.1.4 Effect of Initial Volumetric Flow Rate (Qo)

Figure 18 shows the effect of varying the initial volumetric flow rate from $1x10^{-5}$ to $1x10^{-3}$ m^3/s on the solute concentration and as can be seen the lower the volumetric flow rate, the faster is the rate of decline in the solute concentration, which results in a drastically lower solute concentration. This behavior is due to the longer residence time as well as the ability to interact with large membrane surface area as it travels through it. By lowering the volumetric flow rate, the solute begins to exponentially decrease when compared with the more linear decline at high flow rates.

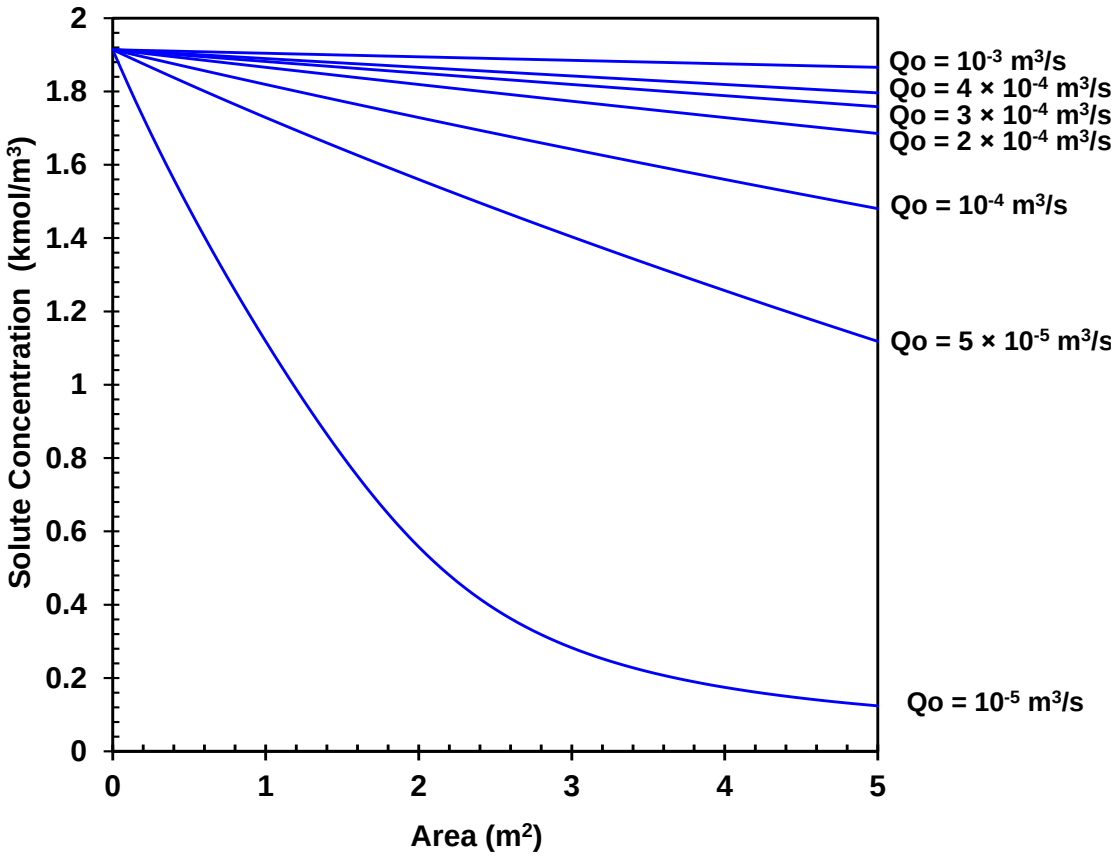

Figure 18: Effect of initial volumetric flow rate on the solute concentration for the RO model

5.1.5 Effect of Membrane Area (A)

Figure 19 shows the effect of changing the membrane area from 1.0 m^2 to 10 m^2 at constant initial flow rate (50 liter/s) on the solute concentration along the length of the reactor. As can be seen in this figure, increasing the membrane area results in a steeper decline in the solute concentration along the length of the reactor at a constant initial flow rate. This behavior is in agreement with Figure 18, where using a large surface area for concentrate diffusion results in a high membrane separation efficiency.

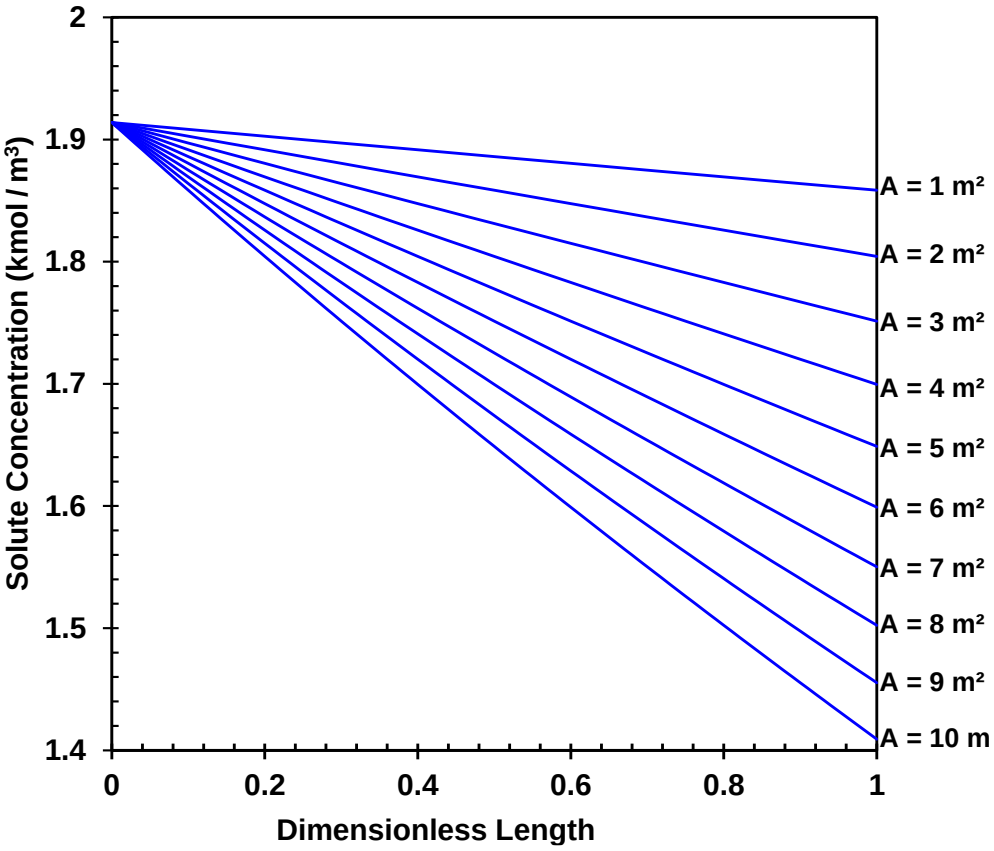

Figure 19: Effect of membrane area on the solute concentration

5.2 SENSITIVITY ANALYSIS FOR NANOFILTRATION PARAMETERS

Similarly, a sensitivity analysis of the factors affecting the nanofiltration (NF) process is conducted. It should be noted that the nanofiltration model is only a function of time.

5.2.1 Effect of Water and Solute Permeability

Figure 20 shows the effect of the water permeability on the change in solute concentration and filtration time in the NF process. The water permeability was varied from 5.5 to 8.5 µm/s at a constant solute permeability of 5 µm/s. As can be seen in this figure increasing the water permeability yielded faster filtration.

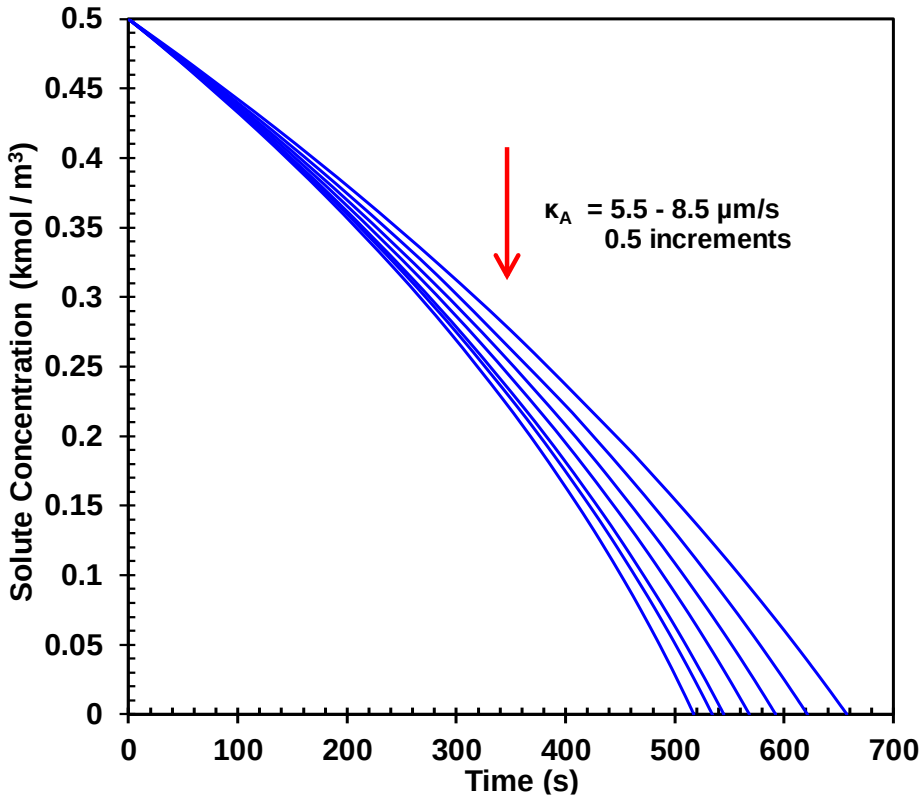

Figure 20: Effect of water permeability on the filtration time for the NF model

Also, Figure 21 shows the effect of the solute permeability, at 3.5, 5 and 6.5 µm/s at a constant water permeability of 7 µm/s on the solute concentration and filtration time. As can be observed in the figure the time to complete filtration decreases with decreasing the solute permeability from 3,5 to 6.5 µm/s.

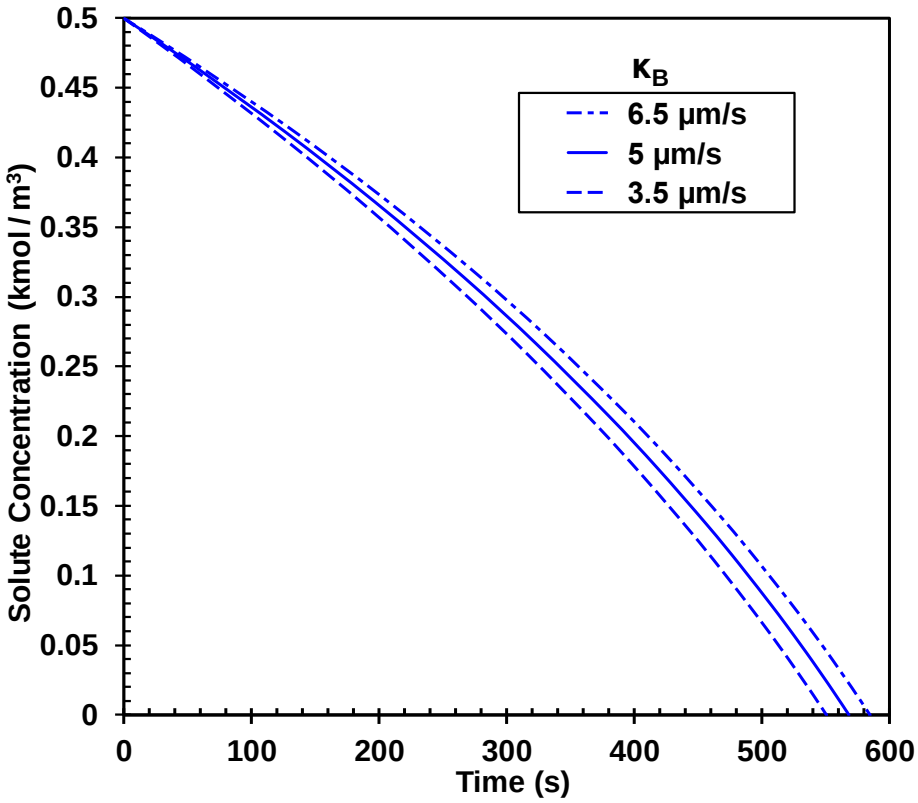

Figure 21: Effect of solute permeability on the filtration time for the NF model

5.2.2 Effect of Pressure Drop

Figure 22 shows the effect of varying the pressure drop across the membrane from 0.2 to 5 MPa on the solute concentration and filtration time; and as can be seen higher pressure drops result in

faster filtration time. It should be noted that increasing the pressure from 0.2 to 2 MPa, significantly decreases the required filtration time by up to 3000 s, whereas increasing the pressure from 2 to 5 MPa decreases the filtration time by only 150 s.

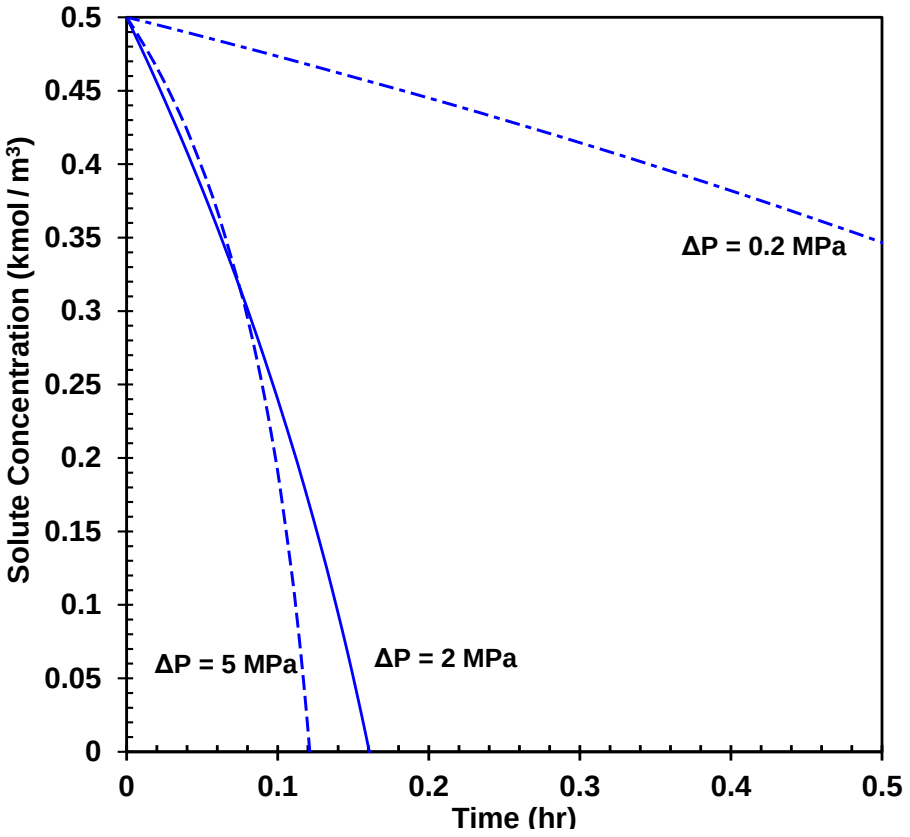

Figure 22: Effect of pressure drop on the filtration time for the NF model

5.2.3 Effect of Reflection Coefficient (σ_o)

Figure 23 shows the effect of varying the reflection coefficient from 0.1 to 1 on the solute concentration and filtration time; and as can be seen increasing the reflection coefficient results in faster filtration times. The reflection coefficient depends on the pressure drop, osmotic pressure,

and concentrations at the permeate and the wall. The reflection coefficient is found from empirical data, and therefore in theory complete rejection can be obtained, but physically this is a difficult target to attain.

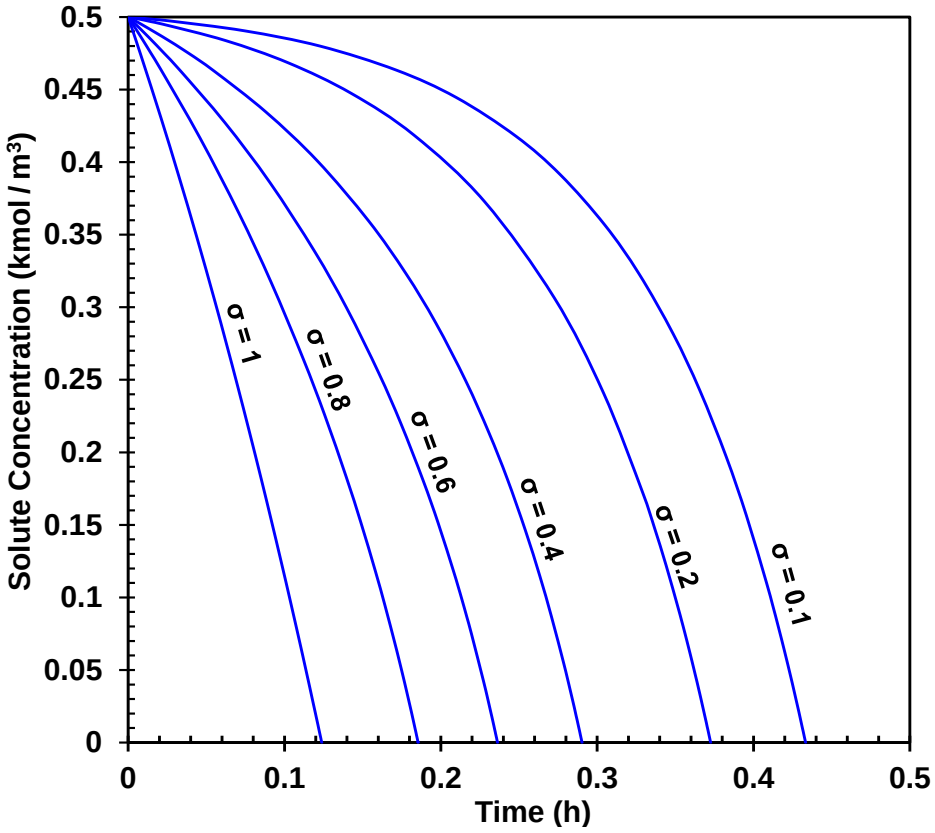

Figure 23: Effect of reflection coefficient on the filtration time for the NF model

5.2.4 Effect of Temperature

Figure 24 shows the effect of varying the process temperature from 275 to 350 K on the solute concentration and filtration time. As can be seen in this figure, faster filtration times are achieved

at lower temperatures, which can be due to the effect of temperature on the osmotic pressure, as shown in Equation (42).

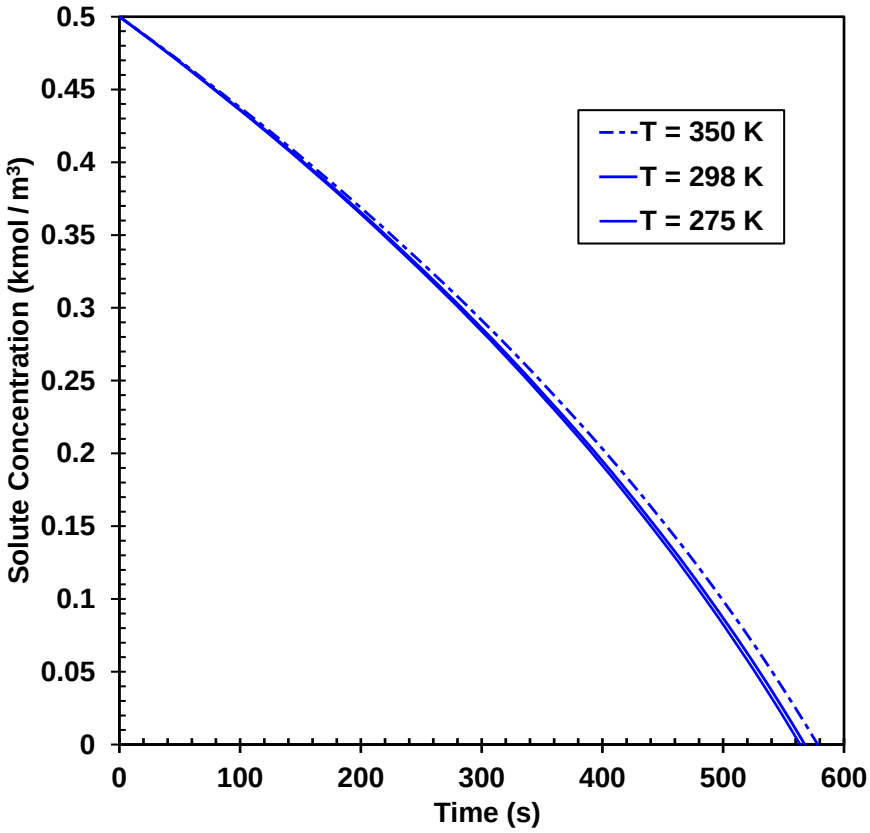

Figure 24: Effect of temperature on the filtration time for the NF model

5.2.5 Effect of Membrane Area (A)

Figure 25 shows the effect of varying the membrane area between 0.2 m^2 and 3.0 m^2 on the solute concentration and filtration time. As can be observed in this figure, a larger membrane area leads to a faster filtration time. This behavior can be due to the increased contact area which allows for more solute to permeate through the membrane. In addition, similar to the behavior exhibited by

the effect of pressure drop, the higher the change in membrane area, the lower the change in filtration time is.

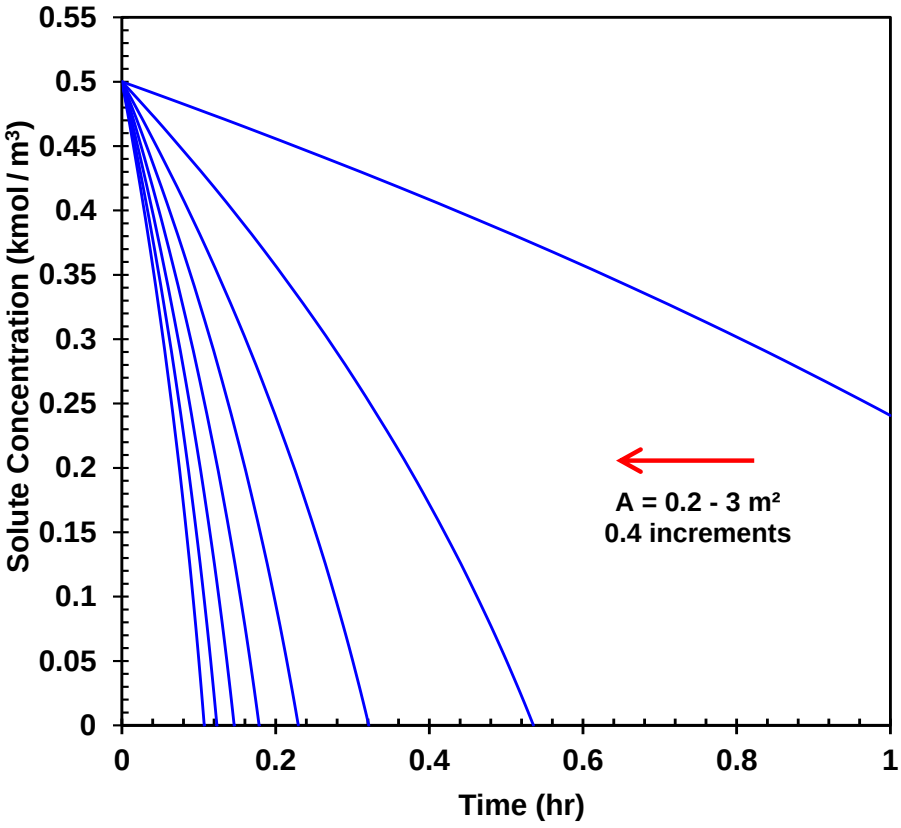

Figure 25: Effect of membrane area on solute concentration for the NF model

5.3 COMPARISON BETWEEN COMMERCIAL MEMBRANES

Four different RO and three different NF membranes with the properties given in Tables 11 and 12, respectively, were compared in terms of their efficiency in the removal of the three main ionic constituents found flowback water (Cl^-, Na^+ and Ca^{2+}). Figure 26 shows the efficiency of the different membranes in removing Cl^-, and as can be seen, nanofiltration membranes have greater removal efficiency of around 15% over that of the RO membranes. This can be explained by the nature of both processes, where reverse osmosis is primarily driven by the chemical potential of chlorine, while nanofiltration is also controlled by the radius of the molecule. It should be mentioned that since chlorine is a relatively large molecule with a relatively weak charge of -1, the effect of the chemical potential on chlorine removal in reverse osmosis is less than the effect of the molecule size in nanofiltration, resulting in a significantly high removal efficiencies in nanofiltration.

Figure 27 shows the efficiency of the different membranes in removing Na^+, and as can be observed the four reverse osmosis membranes exhibit much higher efficiencies of up to 60% over that of the three nanofiltration membranes. This behavior is also due the nature of the driving forces for both processes as discussed in Figure 26. It appears that the effect of the Na^+ chemical potential driving force in reverse osmosis is significantly greater than that of its molecular size in nanofiltration.

A similar effect is also depicted in Figure 28, which shows the efficiency of the different membranes in removing Ca^{2+}. As can be observed the average efficiency of the reverse osmosis membranes are much higher than that of the nanofiltration membranes.

It should be noted that nanofiltration membranes are significantly better in removing Ca^{2+} when compared with the removal of Na^+, which could be due to Ca^{2+} has higher charge than Na^+

and consequently higher chemical potential. On the other hand, reverse osmosis membrane efficiencies for Cl^- were significantly lower than those of Na^+ and Ca^{2+}, which can be attributed to the fact that the concentration of Cl^- is significantly higher in the flowback water when compared with those of Na^+ and Ca^{2+}.

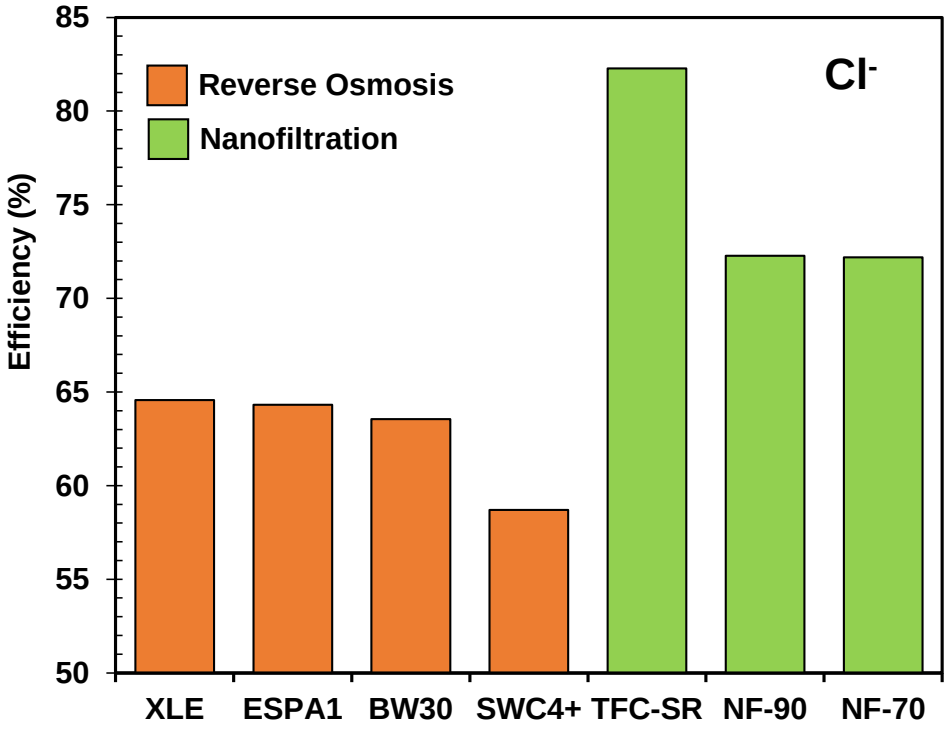

Figure 26: Efficiency of various RO and NF membrane for Cl^- removal

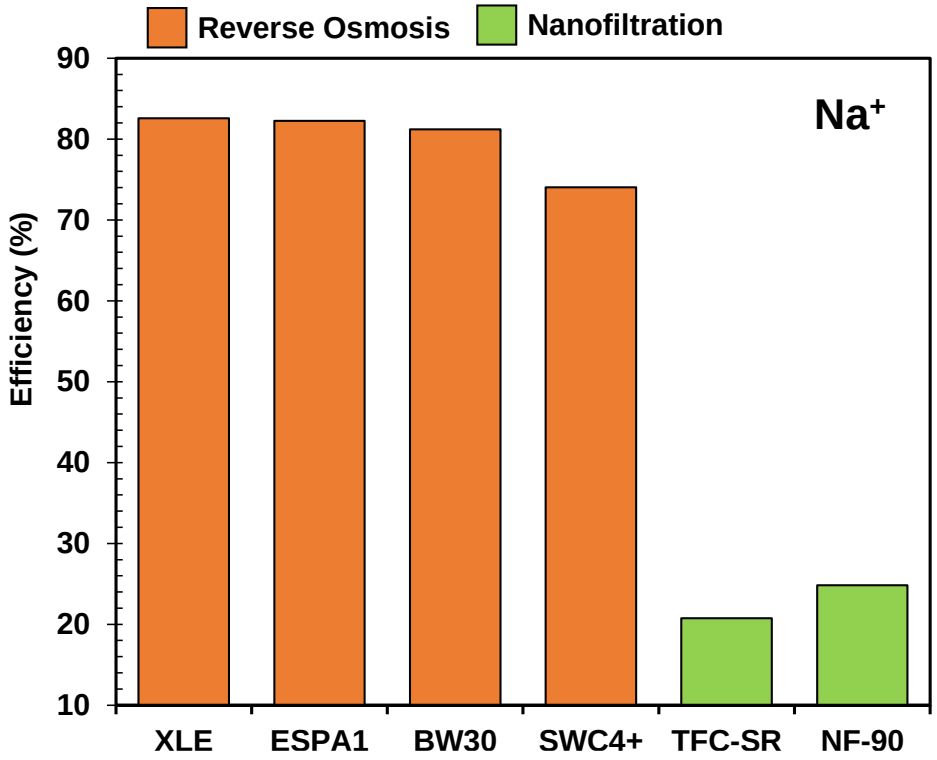

Figure 27: Efficiency of various RO and NF membrane for Na^{+} removal

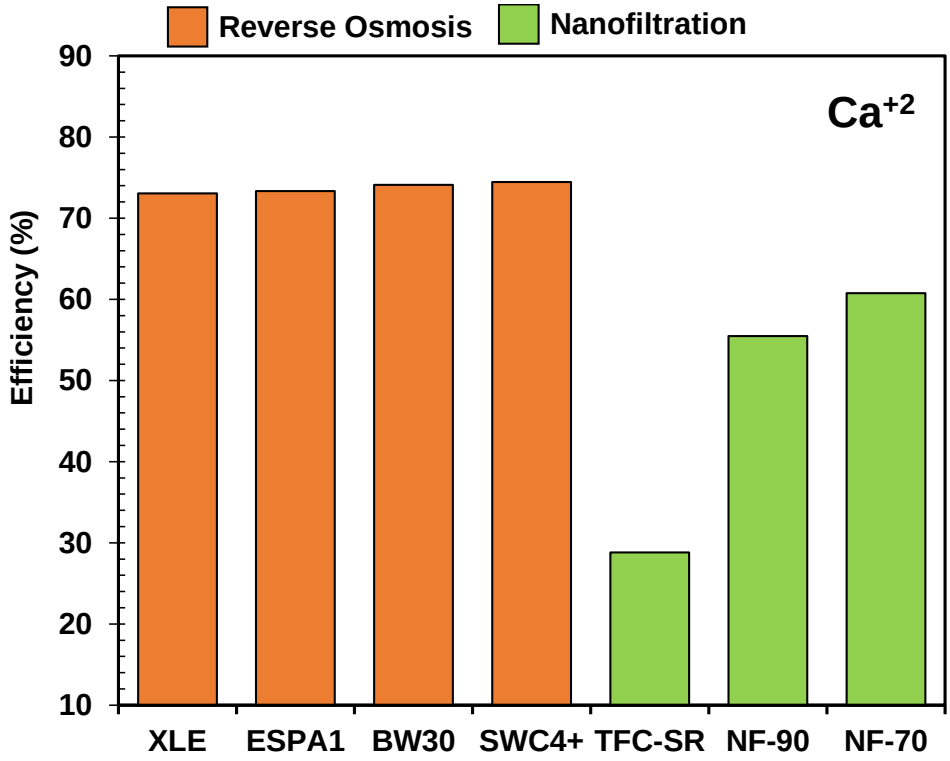

Figure 28: Efficiency of various RO and NF membrane for Ca^{2+} removal

6.0 CONCLUDING REMARKS

- Mathematical models for the reverse osmosis and nanofiltration processes were developed to assess the performance of these processes in the treatment of flowback water produced during the hydraulic fracturing for natural gas production from shale plays. The models, based on the mass balance and thermodynamics, were verified and implemented in Matlab version R2015.
- The models were used to perform a sensitivity analysis for the two processes in order to determine the effect of the operating variables on the membrane performance in terms of solute concentration and filtration time. For the reverse osmosis, it was found that pressure drop, inlet flow rate and membrane area were the major parameters governing the process. For nanofiltration, on the other hand, pressure drop, reflection coefficient and membrane area were the most important parameters affecting the process performance.
- The models were also used to assess and compare the performance of four different commercial reverse osmosis and three nanofiltration membranes using actual filed data, such as inlet flowrate and flowback water composition. The predictions of the two models showed that the reverse osmosis was significantly superior to the nanofiltration membranes in the removal of Na^+ and Ca^+. Nanofiltration membranes, however, exhibited higher removal efficiencies for Cl^- than that of the reverse osmosis membranes. This behavior can be attributed primarily to the nature of both processes; since the reverse osmosis is mainly driven by the chemical potential of chlorine, whereas, the nanofiltration is also controlled by the molecule size.

REFERENCES

[1] A. E. Outlook, "Energy Information Administration," *Department of Energy*, 2014.

[2] K. B. Gregory, R. D. Vidic, and D. A. Dzombak, "Water management challenges associated with the production of shale gas by hydraulic fracturing," *Elements*, vol. 7, pp. 181-186, 2011.

[3] J. D. Arthur, B. K. Bohm, B. J. Coughlin, M. A. Layne, and D. Cornue, "Evaluating the environmental implications of hydraulic fracturing in shale gas reservoirs," in *SPE Americas E&P environmental and safety conference*, 2009.

[4] N. P. Cheremisinoff and A. Davletshin, *Hydraulic fracturing operations: Handbook of environmental management practices*: John Wiley & Sons, 2015.

[5] C. J. Cleveland and C. G. Morris, *Handbook of Energy: Diagrams, Charts, and Tables*: Elsevier Science, 2013.

[6] C. H. Arnaud, "Figuring out Fracking Wastewater," *Chem. Eng. News*, vol. 93, 2015.

[7] A. Granberg. (2008). *What is Hydraulic Fracturing?*

[8] C. Clark and J. Veil, "Produced water volumes and management practices in the United States," Argonne National Laboratory (ANL)2009.

[9] M. D. Holloway and O. Rudd, *Fracking: The Operations and Environmental Consequences of Hydraulic Fracturing*: Wiley, 2013.

[10] D. J. Soeder and W. M. Kappel, *Water resources and natural gas production from the Marcellus Shale*: US Department of the Interior, US Geological Survey Reston, Virginia, 2009.

[11] D. M. Kargbo, R. G. Wilhelm, and D. J. Campbell, "Natural gas plays in the Marcellus shale: Challenges and potential opportunities," *Environmental science & technology*, vol. 44, pp. 5679-5684, 2010.

[12] S. Rassenfoss, "From flowback to fracturing: water recycling grows in the Marcellus shale," *Journal of Petroleum Technology*, vol. 63, pp. 48-51, 2011.

[13] M. McBroom, *The Effects of Induced Hydraulic Fracturing on the Environment: Commercial Demands vs. Water, Wildlife, and Human Ecosystems*: Apple Academic Press, 2013.

[14] A. Vengosh, R. B. Jackson, N. Warner, T. H. Darrah, and A. Kondash, "A critical review of the risks to water resources from unconventional shale gas development and hydraulic fracturing in the United States," *Environmental science & technology,* vol. 48, pp. 8334-8348, 2014.

[15] R. D. Vidic, S. L. Brantley, J. M. Vandenbossche, D. Yoxtheimer, and J. D. Abad, "Impact of shale gas development on regional water quality," *Science,* vol. 340, p. 1235009, 2013.

[16] M. J. Economides and K. G. Nolte, *Reservoir Stimulation*: Wiley, 2000.

[17] M. M. Michel, L. Reczek, M. Granops, P. Rudnicki, and A. Piech, "Pretreatment and desalination of flowback water from the hydraulic fracturing," *Desalination and Water Treatment,* pp. 1-10, 2015.

[18] J.-P. Nicot, B. R. Scanlon, R. C. Reedy, and R. A. Costley, "Source and fate of hydraulic fracturing water in the Barnett Shale: a historical perspective," *Environmental science & technology,* vol. 48, pp. 2464-2471, 2014.

[19] M. E. Blauch, R. R. Myers, T. Moore, B. A. Lipinski, and N. A. Houston, "Marcellus shale post-frac flowback waters-Where is all the salt coming from and what are the implications?," in *SPE Eastern Regional Meeting*, 2009.

[20] C. W. Abdalla, J. Drohan, K. Saacke Blunk, and J. Edson, "Marcellus shale wastewater issues in Pennsylvania: current and emerging treatment and disposal technologies," *Pennsylvania State University, Pennsylvania,* 2011.

[21] T. Hayes, "Sampling and analysis of water streams associated with the development of Marcellus shale gas," *Marcellus Shale Initiative Publications Database,* vol. 10, 2009.

[22] E. Barbot, N. S. Vidic, K. B. Gregory, and R. D. Vidic, "Spatial and temporal correlation of water quality parameters of produced waters from Devonian-age shale following hydraulic fracturing," *Environmental science & technology,* vol. 47, pp. 2562-2569, 2013.

[23] S. Jenkins, "Frac water reuse," *Chemical Engineering,* vol. 119, p. 14, 2012.

[24] M. E. Mantell, "Produced water reuse and recycling challenges and opportunities across major shale plays," in *Proceedings of the technical workshops for the hydraulic fracturing study: water resources management. EPA*, 2011, pp. 49-57.

[25] J. Veil and C. Clark, "Produced water volume estimates and management practices," *SPE Production & Operations,* vol. 26, pp. 234-239, 2011.

[26] O. Dawkins, "Pennsylvania Department of Environmental Protection," T. R. E. Center, Ed., ed, 2008.

[27] S. M. Olmstead, L. A. Muehlenbachs, J.-S. Shih, Z. Chu, and A. J. Krupnick, "Shale gas development impacts on surface water quality in Pennsylvania," *Proceedings of the National Academy of Sciences,* vol. 110, pp. 4962-4967, 2013.

[28] EPA, "National recommended water quality criteria," in *United States Environmental Protection Agency', Office of Water, Office of Science and Technology*, ed, 2009.

[29] D. R. Greenwood, G. Kingsbury, and J. Cleland, *A handbook of key federal regulations and criteria for multimedia environmental control*: US Environmental Protection Agency, Office of Research and Development, 1979.

[30] K. Lee, J. Neff, and E. DeBlois, *Produced water*: Springer, 2011.

[31] T. Hayes and D. Arthur, "Overview of emerging produced water treatment technologies," in *11th Annual International Petroleum Environmental Conference, Albuquerque, NM*, 2004.

[32] E. R. W. Rousseau, *Handbook of separation process technology*: John Wiley & Sons, 2009.

[33] E. T. Igunnu and G. Z. Chen, "Produced water treatment technologies," *International Journal of Low-Carbon Technologies,* p. cts049, 2012.

[34] G. Doran and L. Leong, "Developing a cost effective solution for produced water and creating a 'new'water resource," DOE/MT/95008–4. United Sates Department of Energy2000.

[35] J. Sorensen, J. Boysen, D. Boysen, and T. Larson, "Field Application of the Freeze/Thaw Evaporation (FTE®) Process for the Treatment of Natural Gas Produced Water in Wyoming," ed, 2002.

[36] W. T. Hess, A. Kurtz, and D. Stanton, "Kirk-Othmer encyclopedia of chemical technology," *John Wiley & Sons Ltd., New York,* 1995.

[37] J. Kucera, *Reverse osmosis: design, processes, and applications for engineers*: John Wiley & Sons, 2015.

[38] S. Judd and B. Jefferson, *Membranes for industrial wastewater recovery and re-use*: Elsevier, 2003.

[39] J. Wijmans and R. Baker, "The solution-diffusion model: a review," *Journal of membrane science,* vol. 107, pp. 1-21, 1995.

[40] G. Foley, *Membrane Filtration: A Problem Solving Approach with MATLAB*: Cambridge University Press, 2013.

[41] P. Atkins and J. de Paula, *Atkins' Physical Chemistry*: OUP Oxford, 2010.

[42] L. Dresner, "Some remarks on the integration of the extended Nernst-Planck equations in the hyperfiltration of multicomponent solutions," *Desalination,* vol. 10, pp. 27-46, 1972/02/01 1972.

[43] T. Tsuru, S.-i. Nakao, and S. Kimura, "Calculation of Ion Rejection by Extended Nernst–Planck Equation with Charged Reverse Osmosis Membranes for Single and Mixed Electrolyte Solutions," *JOURNAL OF CHEMICAL ENGINEERING OF JAPAN,* vol. 24, pp. 511-517, 1991.

[44] M. Gräbner, *Industrial Coal Gasification Technologies Covering Baseline and High-Ash Coal*: Wiley, 2014.

[45] Y. Garba, S. Taha, N. Gondrexon, and G. Dorange, "Ion transport modelling through nanofiltration membranes," *Journal of Membrane Science,* vol. 160, pp. 187-200, 7/22/ 1999.

[46] A. Szymczyk, C. Labbez, P. Fievet, A. Vidonne, A. Foissy, and J. Pagetti, "Contribution of convection, diffusion and migration to electrolyte transport through nanofiltration membranes," *Advances in Colloid and Interface Science,* vol. 103, pp. 77-94, 3/19/ 2003.

[47] X.-L. Wang, T. Tsuru, S.-i. Nakao, and S. Kimura, "The electrostatic and steric-hindrance model for the transport of charged solutes through nanofiltration membranes," *Journal of Membrane Science,* vol. 135, pp. 19-32, 11/12/ 1997.

[48] T. U. Kim, "Transport of Organic Micropollutants Through Nanofiltration (NF) and Reverse Osmosis (RO) Membranes: Mechanisms, Modeling, and Applications," University of Colorado at Boulder, 2006.

[49] C. Labbez, P. Fievet, A. Szymczyk, A. Vidonne, A. Foissy, and J. Pagetti, "Retention of mineral salts by a polyamide nanofiltration membrane," *Separation and Purification Technology,* vol. 30, pp. 47-55, 1// 2003.

[50] W. R. Bowen, A. W. Mohammad, and N. Hilal, "Characterisation of nanofiltration membranes for predictive purposes — use of salts, uncharged solutes and atomic force microscopy," *Journal of Membrane Science,* vol. 126, pp. 91-105, 4/2/ 1997.

[51] P. Fievet, C. Labbez, A. Szymczyk, A. Vidonne, A. Foissy, and J. Pagetti, "Electrolyte transport through amphoteric nanofiltration membranes," *Chemical Engineering Science,* vol. 57, pp. 2921-2931, 8// 2002.

[52] N. Voros, Z. Maroulis, and D. Marinos-Kouris, "Salt and water permeability in reverse osmosis membranes," *Desalination,* vol. 104, pp. 141-154, 1996.

[53] E. Dražević, K. Košutić, and V. Freger, "Permeability and selectivity of reverse osmosis membranes: Correlation to swelling revisited," *Water research,* vol. 49, pp. 444-452, 2014.

[54] H. Krieg, S. Modise, K. Keizer, and H. Neomagus, "Salt rejection in nanofiltration for single and binary salt mixtures in view of sulphate removal," *Desalination*, vol. 171, pp. 205-215, 2005.